

Supporting Information

Theoretical Study of One-Electron-Oxidized Salen Complexes of Group 7 (Mn(III), Tc(III), and Re(III)) and Group 10 Metals (Ni(II), Pd(II), and Pt(II)) with 3D-RISM-GMC-QDPT Method: Localized vs. Delocalized Ground and Excited States in Solution

Shinji Aono, Masayuki Nakagaki, and Shigeyoshi Sakaki*

*Fukui Institute for Fundamental Chemistry, Kyoto University, Nishihiraki-cho, Takano, Sakyo-ku,
Kyoto 606-8103, Japan*

E-mail: sakaki.shigeyoshi.47e@st.kyoto-u.ac.jp

*To whom correspondence should be addressed

Details of RISM-SCF method

In the RISM-SCF method,¹³ electronic structure of solute is calculated in the presence of equilibrium solvent distribution about the solute based on the statistical mechanics of liquid.^{14,15} In the 1D-RISM-SCF method, the solvation structure was represented by the radial distribution function of solvent site, which was determined by solving Ornstein-Zernike integral equation with 1D closure equation. Analytical gradient of the 1D-RISM-SCF free energy was evaluated under the variational principle¹⁶ which has been employed to determine the solute geometries and free energy profiles of chemical reactions in solution. The RISM integral equation has been extended by many researchers based on the density functional theory of non-uniform polyatomic liquid proposed by Chandler *et al.*¹⁷ For instance, Beglov and Roux applied the 3D hyper-netted chain (HNC) equation to the distribution of mono-atomic Lennard-Jones (LJ) solvent¹⁸ and the 3D-RISM-HNC theory to the solvation of polar molecules in aqueous phase;^{19,20} Kovalenko and Hirata derived the 3D generalization of the RISM method from the six-dimensional (6D) molecular Ornstein-Zernike integral equation, where the rotational degrees of freedom of solvent were averaged out,²¹⁻²² and combined it with the electronic structure calculations.²³ In the 3D-RISM-SCF method, the equilibrium solvent distribution can be represented by probability density function of solvent site at the 3D grid space around the solute molecule, which provides direct information about the solvation structure. Analytical gradient of the 3D-RISM-SCF free energy was also derived and then full geometry optimization of the solute molecule was performed at both the DFT and HF levels under consideration of solvation effect.^{24,25} Because, in the 3D-RISM-SCF method, the point-charge approximation of the solute molecule is not always necessary to evaluate electrostatic potential (ESP) around the solute molecule, which determines the equilibrium solvent distribution, the direct evaluation of ESP by the one-electron integral improved the description of solvation structure near the solute molecule in accuracy and SCF convergence.²⁵ In this work, the full geometry optimization was performed by the three-regions 3D-RISM-SCF method,²⁶ which is the modification of Ref. [25].

The complete description of reference [40] in the main text is, as follows:

M. W. Schmidt, K. K. Baldrige, J. A. Boatz, S. T. Elbert, M. S. Gordon, J. H. Jensen, S. Koseki, N. Matsunaga, K. A. Nguyen, S. Su, T. L. Windus, M. Dupuis, J. A. Montgomery, *J. Comput. Chem.*, General Atomic and Molecular Electronic Structure System. *J. Comput. Chem.*, 1993, **14**, 1347-1363.

The complete description of reference [41] in the main text is, as follows:

GAUSSIAN 09, Revision B.01, M. J. Frisch, G. W. Trucks, H. B. Schlegel, G. E. Scuseria, M. A. Robb, J. R. Cheeseman, G. Scalmani, V. Barone, B. Mennucci, G. A. Petersson, H. Nakatsuji, M. Caricato, X. Li, H. P. Hratchian, A. F. Izmaylov, J. Bloino, G. Zheng, J. L. Sonnenberg, M. Hada, M. Ehara, K. Toyota, R. Fukuda, J. Hasegawa, M. Ishida, T. Nakajima, Y. Honda, O. Kitao, H. Nakai, T. Vreven, J. A. Montgomery, Jr., J. E. Peralta, F. Ogliaro, M. Bearpark, J. J. Heyd, E. Brothers, K. N. Kudin, V. N. Staroverov, T. Keith, R. Kobayashi, J. Normand, K. Raghavachari, A. Rendell, J. C. Burant, S. S. Iyengar, J. Tomasi, M. Cossi, N. Rega, J. M. Millam, M. Klene, J. E. Knox, J. B. Cross, V. Bakken, C. Adamo, J. Jaramillo, R. Gomperts, R. E. Stratmann, O. Yazyev, A. J. Austin, R. Cammi, C. Pomelli, J. W. Ochterski, R. L. Martin, K. Morokuma, V. G. Zakrzewski, G. A. Voth, P. Salvador, J. J. Dannenberg, S. Dapprich, A. D. Daniels, O. Farkas, J. B. Foresman, J. V. Ortiz, J. Cioslowski, D. J. Fox, Gaussian, Inc., Wallingford CT, 2010.

Geometry and Electronic Structure of Non-oxidized Metal-Salen Complexes

Geometry and electronic structure of non-oxidized salen complexes of group 7 and 10 metals in CH₂Cl₂ solution are calculated by 3D-RISM-SCF-U-DFT method with the M06 functional; see electronic supporting information (ESI) Tables S3-S5 for geometrical parameters, the electron configurations, and the spin populations and charges on **M** and salen ligand.^{S1,S2} In **2ⁿa**, **4ⁿa**, **5ⁿa**, and **6ⁿa**, the ground state is closed-shell singlet but in **1ⁿa** and **3ⁿa** the ground state is quintet consisting of four β -spin SOMOs, the **M** d_{xz} , d_{yz} , d_{z^2} , and $d_{x^2-y^2}$ orbitals.

In non-oxidized **1ⁿ** and **3ⁿ**, the ground state is quintet; for instance, the quintet state of **1ⁿa** and **3ⁿa** are more stable than the triplet state by 30.8 and 8.2 kcal mol⁻¹ and the closed-shell singlet state by 74.6 and 11.7 kcal mol⁻¹, respectively, in CH₂Cl₂ solution, as shown in Table S3. This means that energy difference between the quintet state and next stable state is smaller in **3ⁿa** than in **1ⁿa**. In Re(III) complex **5ⁿ**, the ground state is closed-shell singlet; for instance, the closed-shell singlet state of **5ⁿa** is more stable than the triplet state by 1.7 kcal mol⁻¹ and the quintet state by 7.7 kcal mol⁻¹. Hence, one of the most important features in the non-oxidized salen complexes of group 7 metals is that four d electrons of Re(III) takes low-spin state unlike those of Mn(III) and Tc(III), indicating that the d orbital energy splitting is larger in the Re(III) complex than in the Mn(III) and Tc(III) complexes; this feature is observed by the d orbital energies of α -spin unoccupied MOs in the quintet state and the d orbital energy splitting increases in the order Mn(III) < Tc(III) < Re(III), as shown in Figure S3 in ESI.

As shown in Table S4 in ESI, the triplet state of **1ⁿa** suffers from the large spin contamination^{S3} unlike in all other complexes, indicating that in **1ⁿa** the relative stability of the triplet state (30.8 kcal mol⁻¹) is overestimated because of the mixing of very stable quintet state. Considering that the triplet state is not the lowest energy state of **1ⁿa** despite the overestimation of stability, the spin contamination does not change the conclusion that the ground state of **1ⁿa** is not double but quintet like that of **3ⁿa** at the U-DFT level.

In most spin states, the non-oxidized salen complexes of group 7 and 10 metals take the C₂-symmetrical geometry with the delocalized electronic structure except for the triplet state of **1ⁿa**,

which does not seem correct feature because of the large spin contamination, as mentioned above. The radical character on the salen ligand is small in the Mn(III) complex but becomes larger in the Tc(III) and Re(III) complexes, as shown in Table S5 in ESI, because the orbital mixing between the $\mathbf{M} d_{xz}$ orbital and the salen π_a orbital significantly increases when going from the first-row transition metal element to the third-row one.

The $\mathbf{M-O}$ and $\mathbf{M-N}$ bond lengths are the shortest in the complexes of the first-row transition metal elements $\mathbf{1}^n\mathbf{a}$ and $\mathbf{2}^n\mathbf{a}$ but become moderately longer in those of the second-row transition metal elements $\mathbf{3}^n\mathbf{a}$ and $\mathbf{4}^n\mathbf{a}$ than in those of the third-row transition metal elements $\mathbf{5}^n\mathbf{a}$ and $\mathbf{6}^n\mathbf{a}$, as shown in Table S3. In the non-oxidized salen complexes of group 7 metals, both of the singlet and quintet states exhibit the same trend, as follows: In the singlet state, the $\mathbf{M-O}$ distance increases in the order $\mathbf{1}^n\mathbf{a}$ (1.71 Å) < $\mathbf{5}^n\mathbf{a}$ (1.82 Å) < $\mathbf{3}^n\mathbf{a}$ (1.87 Å) and the $\mathbf{M-N}$ distance increases in the order $\mathbf{1}^n\mathbf{a}$ (1.97 Å) < $\mathbf{5}^n\mathbf{a}$ (2.04 Å) < $\mathbf{3}^n\mathbf{a}$ (2.08 Å). In the quintet state, the $\mathbf{M-O}$ distance increases in the order $\mathbf{1}^n\mathbf{a}$ (1.84 Å) < $\mathbf{5}^n\mathbf{a}$ (1.97 Å) \leq $\mathbf{3}^n\mathbf{a}$ (1.98 Å) and the $\mathbf{M-N}$ distance increases in the order $\mathbf{1}^n\mathbf{a}$ (1.95 Å) < $\mathbf{5}^n\mathbf{a}$ (2.03 Å) < $\mathbf{3}^n\mathbf{a}$ (2.06 Å). Similarly, in the group 10 analogues, the $\mathbf{M-O}$ and $\mathbf{M-N}$ distances are the shortest in the complex of the first-row transition metal element $\mathbf{2}^n\mathbf{a}$ but they are almost the same between those of the second and third transition metals $\mathbf{4}^n\mathbf{a}$ and $\mathbf{6}^n\mathbf{a}$; the $\mathbf{M-O}$ distance increases in the order $\mathbf{2}^n\mathbf{a}$ (1.85 Å) < $\mathbf{6}^n\mathbf{a}$ (2.02 Å) \sim $\mathbf{4}^n\mathbf{a}$ (2.02 Å) and the $\mathbf{M-N}$ distance increases in the order $\mathbf{2}^n\mathbf{a}$ (1.85 Å) < $\mathbf{6}^n\mathbf{a}$ (1.97 Å) \leq $\mathbf{4}^n\mathbf{a}$ (1.98 Å). These results are reasonable because it is well known that the ionic radius of the transition metal becomes longer in general when going from the first-row transition metal element to the second-row one with the same group and the same oxidation state but it changes little when going from the second-row transition metal element to the third-row one; remember that the increase of the principal quantum number usually induces the orbital expansion but the orbital expansion going from the second-row transition metal element to the third-row one does not occur largely because the weak shielding effect of the 4f electron leads to the contraction of orbital radius.

In the non-oxidized salen complexes of group 7 metals, the $\mathbf{M-O}$ distance is much longer in the quintet state than in the closed-shell singlet state by 0.11 - 0.15 Å but the $\mathbf{M-N}$ distance is a

little bit shorter in the quintet state than in the closed-shell singlet state by 0.01 - 0.02 Å, as shown in Table S3. This is reasonable, as follows: Because the **M** d_{xz} SOMO in the quintet state has the anti-bonding combination with the π orbitals on the O site of salen ligand (see the d_{xz} orbitals in Figure S3 in ESI), the **M**-O bond length becomes longer in the quintet state than in the closed-shell singlet state; remember that the d_{xz} orbital is unoccupied in the closed-shell singlet state. The other reason is that the electrons of the d_{z^2} and d_{yz} orbitals, which are doubly occupied in the closed-shell singlet state, exhibit a weak shielding effect on the x -direction of the salen ligand (in other words, the ESP on the x -direction of the salen ligand becomes more positive in the closed-shell singlet state than in the quintet state) and hence the electrostatic attraction between the positively charged **M** and the negatively-charged O sites of the salen ligand becomes larger in the closed-shell singlet state than in the quintet state.

The relative stability of spin states and the **M**-O and **M**-N bond lengths largely depend on the kinds of the central metal **M**, as mentioned above. These features of the non-oxidized metal-salen complexes deeply relate to those of the one-electron oxidized metal-salen complexes, as shown in the main text.

[S1]: Glendening, E. D.; Badenhop, J. K.; Reed, A. E.; Carpenter, J. E.; Bohmann, J. A.; Morales, C. M.; Weinhold, F. NBO 5.0. Theoretical Chemistry Institute, University of Wisconsin, Madison, 2001.

[S2]: The orbital mixing between the **M** d_{xz} orbital and the salen π_b orbital becomes much larger when going from the first-row transition metal element to the third-row one. Hence, in the quintet state, the β -spin population decreases on **M** and increases on the salen ligand when going from the first-row transition metal element to the third-row one, as shown in Table S5 in ESI.

[S3]: The U-DFT calculation also induced the large spin contamination in the singlet state of Mn(III) complex **1a** and provided the open-shell singlet state geometry as the free energy minimum; note that the closed-shell singlet state geometry was found as the free energy minimum in the Tc(III) and Re(III) complexes **3ⁿa** and **5ⁿa**.

The Lowest Energy Quartet Excited State of One-Electron Oxidized Salen Complexes of Re(III)

For comparison of the Re(III) complex with the Mn(III) and Tc(III) analogues, we investigated the quartet state of the Re(III) complex here. As discussed in Section 4.3, the absence of spin population on the salen ligand and essentially the same geometry of the salen as that of the non-oxidized complex indicate that one-electron oxidation occurs mainly on the Re center in the lowest energy quartet state unlike in **1** and **3**, in which one-electron oxidation occurs on the salen ligand. As will be discussed in pages S16-S19, the α - and β -spin electrons of **5** occupy the $a_1\pi_a + b_2d_{xz}$ and $b_2\pi_a + a_2d_{xz}$ MOs, respectively, at the U-DFT level, where the LCAO coefficients are $a_1 \geq b_1$ and $a_2 \geq b_2$. This means that, in the spin restricted picture, the main configuration $(a\pi_a + bd_{xz})^2(d_{yz})^\beta(d_{z^2})^\beta(d_{x^2-y^2})^\beta$ largely undergoes the mixing of the $(a\pi_a + bd_{xz})^\alpha(ad_{xz} - b\pi_a)^\beta(d_{yz})^\beta(d_{z^2})^\beta(d_{x^2-y^2})^\beta$ in the lowest energy quartet state of **5**, which does not correspond to one-electron oxidation of salen π MO but to that of delocalized MO consisting of d_{xz} and π_a MOs; see pages S16-S19 for details. Also, note that the anti-bonding $ad_{xz} - b\pi_a$ orbital exists at much higher energy than the bonding $a\pi_a + bd_{xz}$ one in **5**.

In this quartet state, we must consider the electron configuration consisting of a closed-shell singlet electron configuration of $[\text{salen}]^{2-}$ and a quartet electronic structure of Re(IV) with three β -spin d_{z^2} , d_{yz} , and $d_{x^2-y^2}$ SOMOs. This electron configuration is not included in the 2SA-GMC-QDPT(LAS/MAS) and 2SA-GMC-QDPT(SAS/SAS). However, the SA-GMC-QDPT calculation including the excited state corresponding to above-mentioned electron configuration could not be performed at the LAS/MAS level due to huge computational cost. Here, we employed the three-state averaged GMC-QDPT(SAS/SAS) method (named "3SA-GMC-QDPT(SAS/SAS)") for the lowest energy quartet states (Scheme 4); see Ref. [S4] for details of the parent determinants. This is reasonable because the 2SA-GMC-QDPT(SAS/SAS)-calculated results are essentially the same as those of the 2SA-GMC-QDPT(LAS/MAS); see Table 2 in the main text and page S11 and Table S13 in ESI.

The excitation energy ΔE , the oscillator strength f , and the dipole moment μ_x are shown in

Table S14 in ESI. The 3SA-GMC-QDPT(SAS/SAS) calculations provided the reasonable results that the above-mentioned electron configuration has the largest weight (about 60 %) in the lowest energy quartet state. In the second largest electron configuration whose weight is 20 %, the quintet state of the Re(III) induces the low-spin coupling with the doublet state of the salen radical consisting of the π_a SOMO in **5a** and **5b** and the π_1 SOMO in **5c**. This main configuration is similar to the electronic structure provided by the U-DFT calculation with the M06 functional, indicating that the U-DFT/M06-optimized geometry is reasonable. In the first excited state, the main configuration with weight of about 80 % consists of a quintet state of the Re(III) which induces the low-spin coupling with the π_b SOMO of the salen radical ligand in **5a** and **5b** and the π_2 SOMO in **5c**. The second excited state consists of the same electron configurations as those of the lowest energy quartet state, while the phase of CI coefficients of the second excited state is reverse to that of the lowest energy quartet state. Hence, in **5a** and **5b**, the first excitation exhibits very large oscillator strength but the second excitation does very small one.^{S5}

These results indicate that the first excitation is the $\pi_b \rightarrow d_{xz}$ transition with the large oscillator strength and the second excitation is the $\pi_a \rightarrow d_{xz}$ transition with the small oscillator strength in the quartet state of **5**. These excitations differ from those of **1** and **3** in which the first excitation is the $\pi \rightarrow \pi$ transition with the large oscillator strength in the quartet ground state. In gas phase, the 3SA-GMC-QDPT(SAS/SAS)-calculated excitation to the first excited $\pi_b \rightarrow d_{xz}$ state is calculated at 1.46 eV for **5a** and 1.30 eV for **5b**, which is the lowest energy allowed transition of **5** in the quartet state, and the second excitation ($\pi_a \rightarrow d_{xz}$) is calculated at 2.16 eV for **5a** and 2.12 eV for **5b**. The former energies are much higher than those (0.73 eV for **1a**, 0.38 eV for **1b**, 0.58 eV for **3a**, and 0.42 eV for **3b**) of the $\pi_b \rightarrow \pi_a$ excitation calculated by the 2SA-GMC-QDPT(SAS/SAS), which is the lowest energy allowed transition in **1a**, **1b**, **3a** and **3b**. In weakly polar solvent, the excitation energy of **5** is still larger than those of **1** and **3**; in CH₂Cl₂ solution, they are calculated to be 1.11 eV for **1a**, 0.70 eV for **3a**, and 1.49 eV for **5a**, which agree with those (0.80 eV for **1a**, 0.70 eV for **3a**, and 1.21 eV for **5a**) calculated by the U-TDDFT/M06 (Table S2 in ESI).^{S6} In strongly polar H₂O solvent, however, the excitation energy of **5** becomes lower than that of **1** because the

$\pi \rightarrow d_{xz}$ excitation energy of **5** does not increase so much by the solvation effect unlike the $\pi \rightarrow \pi$ excitation energy of **1** and **3**.

In **5** with the symmetrical salen ligand ($R^1 = R^2$), the excitation from the first $\pi_b \rightarrow d_{xz}$ excited state to the second $\pi_a \rightarrow d_{xz}$ one can be considered as the $\pi_a \rightarrow \pi_b$ transition from the $(\pi_b)^\alpha(\pi_a)^2(d_{xz})^\beta(d_{yz})^\beta(d_{z^2})^\beta(d_{x^2-y^2})^\beta$ quartet state, the absorption spectrum of which cannot be experimentally observed even if the quartet state of **5** is detected because it is not the excitation from the lowest energy quartet state. Also, this excitation does not correspond to the lowest energy allowed $\pi_b \rightarrow \pi_a$ excitation of **1** and **3** but the $\pi_a \rightarrow \pi_b$ one. This discrepancy is surprising; actually, the 2SA-GMC-QDPT(LAS/MAS) and 2SA-GMC-QDPT(SAS/SAS) calculations under the C_2 symmetry provided the above-mentioned $\pi_a \rightarrow \pi_b$ excitation in **5**, while it provided the $\pi_b \rightarrow \pi_a$ excitation in **1**, **2**, **3**, **4**, and **6**.

Based on these results, it is concluded that the electron configuration consisting of a closed-shell singlet electron configuration of $[\text{salen}]^{2-}$ and a quartet configuration of Re(IV) with the d_{z^2} , d_{yz} , and $d_{x^2-y^2}$ SOMOs is important in the lowest energy quartet state of the Re(III) complexes unlike in those of Tc(III) and Mn(III) complexes; remember that 3SA-GMC-QDPT(SAS/SAS) contains this electron configuration in the parent determinants but 2SA-GMC-QDPT(SAS/SAS) does not (Scheme 4 in the main text), indicating that 2SA-GMC-QDPT(SAS/SAS) is not useful for investigating the quartet state of **5**. In such quartet state, **5** has +IV oxidation state of Re and no mixed-valence nature unlike **1** and **3** which have +III oxidation state of **M** and mixed-valence nature.

[S4]: We performed the three-state averaged GMC-QDPT calculation to investigate the lowest energy quartet state of the one-electron oxidized Re(III)-salen complex, in which three parent determinants were considered to describe the main configurations consisting of such states as $(\pi_b)^\alpha(\pi_a)^2(d_{xz})^\beta$, $(\pi_b)^2(\pi_a)^\alpha(d_{xz})^\beta$, and $(\pi_b)^2(\pi_a)^2(d_{xz})^0$ in the C_2 symmetrical structure, as shown in Scheme 4 in the main text; note that π_a and π_b change to π_1 and π_2 , respectively, in the asymmetrical C_1 structure. Then, we constructed the CI space by allowing single and double excitations

from the three parent determinants to the excited determinants. This three-state averaged GMC-QDPT calculation with the SAS and above-mentioned CI space is hereafter named “3SA-GMC-QDPT(SAS/SAS)”.

[S5]: By considering the symmetry of the MOs, it is easy to understand the transition dipole moment in the x -direction is large in the first excitation but very small in the second one. Because the d_{xz} , π_a , and x belong to the irreducible representation B and the π_b belongs to the representation A, $\langle d_{xz} | x | \pi_b \rangle$ and $\langle \pi_a | x | \pi_b \rangle$ are large but $\langle d_{xz} | x | d_{xz} \rangle$ and $\langle \pi_a | x | \pi_a \rangle$ are negligibly small. The former two integrals do not contribute to the transition dipole moment of the second excitation but contribute to that of the first excitation.

[S6]: Also, the U-TDDFT/M06 calculation provides the $\pi \rightarrow \pi$ excitation as the lowest energy excitation in **1** and **3** but provides the $d \rightarrow d$ excitations at lower energy than the $\pi \rightarrow d_{xz}$ excitation in **5**, suggesting that the lowest energy quartet state of **5** differs in character from those of **1** and **3**.

Reliability of GMC-QDPT(SAS/SAS) Computational Results

As shown in Table S13 in ESI, the 3D-RISM-2SA-GMC-QDPT(SAS/SAS) calculation provided the similar result to the 3D-RISM-2SA-GMC-QDPT(LAS/MAS)-calculated one (Table 2 in the main text), indicating that the active space was reasonably taken here even by the SA-GMC-QDPT method with the SAS CI space. For instance, in the one-electron oxidized salen complexes of group 10 metals, $\Delta E_{\text{sol}}^{\text{avg}}$ values of **2a**, **2b**, **2c**, **4a**, and **6a** in CH_2Cl_2 solution are calculated to be 0.49, 0.45, 1.47, 0.41, and 0.64 eV, respectively, which agree with the experimental values of 0.62, 0.58, 0.89, 0.51, and 0.68 eV. In the group 7 analogues, the $\Delta E_{\text{sol}}^{\text{avg}}$ values of **1a**, **1b**, and **1c** in CH_2Cl_2 solution are calculated to be 1.11, 1.13, and 1.70 eV, respectively, which agree with the experimental values of 0.84, 0.98, and 1.39 eV. These 3D-RISM-2SA-GMC-QDPT(SAS/SAS)-calculated results agree with the experimental observation that the vertical excitation energy in CH_2Cl_2 solution increases in the orders **1a** < **1b** \ll **1c**, **2b** < **2a** \ll **2c**, and **4a** < **2a** < **6a** like in the 3D-RISM-2SA-GMC-QDPT(LAS/MAS)-calculated results.

The above-mentioned results indicate that the SA-GMC-QDPT(SAS/SAS) method with the SAS CI space is useful to discuss the localization/delocalization character of the one-electron oxidized salen complexes of group 7 and 10 metals. Hence, in Section 4.3, we investigated the excitations of Re(III) complexes with the ground state by the SA-GMC-QDPT calculation with the small CI space ("SAS2" in the main text) similar to that of the 2SA-GMC-QDPT(SAS/SAS).

Spin Distribution in Doublet State of One-electron Oxidized Salen Complexes of Group 10 Metals.

We will discuss here how the NBO spin distribution changes in the one-electron oxidized salen complexes of group 10 metals **2a**, **4a**, and **6a** at the U-DFT level when going from the first-row transition metal element to the third-row one in the doublet ground state.

As shown in Table S15 in ESI, the salen π orbitals have large spin population of about 0.8 - 0.9 e and the **M** d_{xz} orbital has remaining spin population of about 0.1 - 0.2 e in gas phase and weakly polar solvent. The sum of the spin populations on the (PhO+CN)¹ and (PhO+CN)² moieties depends little on the kinds of **M** and solvent. The sum of the charges on these two moieties differs little, too; see Table S16 in ESI. Also, it is noted that the spin population and charge are the same between the (PhO+CN)¹ and (PhO+CN)² moieties at the C_2 -symmetrical geometry, which reflects the delocalized electronic structure, as shown in Figure S5a in ESI. However, those of (PhO+CN)¹ and (PhO+CN)² moieties differ largely in polar solvent (CH₃OH and H₂O), depending on the kinds of **M**. In the Ni(II) complex **2a**, the geometry distorts from the C_2 -symmetry to the asymmetrical C_1 and the spin population is more positive on the (PhO+CN)² moiety than on the (PhO+CN)¹ in strongly polar H₂O solvent but such geometrical distortion does not occur in CH₃OH solution, as shown in Figure S5b and Table S15 in ESI. In the Pd(II) complex, the geometrical distortion occurs in both of CH₃OH and H₂O solutions. In the Pt(II) complex, on the other hand, it does not occur in both solutions. These results indicate that the tendency for taking a delocalized electronic structure increases in the order Pd(II) < Ni(II) < Pt(II).

To make clear the influences of the geometrical distortion, we performed the NBO analysis, assuming the C_2 -symmetry for comparison; see values in parentheses in Tables S15-S17 in ESI for the total spin populations, charges, and α - and β -spin populations. When going from **2a** to **4a** under the C_2 -symmetry, the sum of the spin populations on the (PhO+CN)¹ and (PhO+CN)² moieties changes little but the sum of their charges becomes more positive by 0.14 e , indicating that the CT from the salen ligand to **M** is larger in **4a** than in **2a** by 0.07 e on both of the α - and β -spin spaces. Both α - and β -spin populations on the **M** d_{xy} orbital are larger in **4a** than in **2a** by

0.08 e , while those of other **M** d orbitals differ little between α - and β -spins, as shown in Table S17. This means that both σ -donations of α - and β -spins are larger in **4a** than in **2a**. Judging from the changes in the **M**-O and **M**-N bond orders (Table S18A in ESI), the σ -donation from the N sites of salen ligand is larger in **4a** than in **2a** but that from the O sites of salen ligand is a little bit smaller.

In gas phase and weakly polar solvent, **2a** and **4a** have delocalized electronic structure but in strongly polar solvent they have localized electronic structure; see that the spin population becomes more negative on the (PhO+CN)¹ moiety by 0.24 e in **2a** and 0.28 e in **4a** and more positive on the (PhO+CN)² moiety by 0.24 e in **2a** and 0.31 e in **4a**, when going from the C_2 -symmetrical geometry to the asymmetrical C_1 in strongly polar H₂O solvent. These results indicate that the orbital mixing occurs between the π_a and π_b orbitals to provide the localized π_1 and π_2 orbitals and one α -spin electron occupies an MO at lower energy.

When going from **4a** to **6a**, the sum of the spin populations on the (PhO+CN)¹ and (PhO+CN)² moieties becomes more negative by 0.11 e and the sum of their charges becomes more negative by 0.15 e , indicating that the β -spin population somewhat increases on the salen ligand by 0.13 e but the α -spin population increases on the salen ligand by only 0.02 e . This is reasonable because the orbital mixing of the **M** d_{xz} orbital with the salen π_a orbital becomes larger in the order Ni(II) < Pd(II) < Pt(II) in the β -spin lowest unoccupied MO (LUMO), as shown in Figure S6. Because the bonding and anti-bonding MOs between the **M** d_{xz} orbital and the salen π_a orbital share two α -spin electrons and one β -spin electron, the enhancement of the orbital mixing of the π_a with the **M** d_{xz} decreases the β -spin population on **M** and increases it on the salen ligand but changes little the α -spin distribution. Therefore, the β -spin population of the **M** d_{xz} orbital is smaller in **6a** than in **4a** by 0.10 e , as shown in Table S17 in ESI. The orbital energy of β -spin LUMO is similar between **2a** and **4a** but the β -spin LUMO of **6a** exists at higher energy than those of **2a** and **4a** by 0.08 eV, as shown in Figure S6, indicating that the orbital mixing is larger in **6a** than in **2a** and **4a**. The large orbital mixing enhances the Pt-O and Pt-N bond orders, as shown in Table S18A in ESI. Also, the geometry of **6a** does not change to C_1 -symmetry even in strongly polar solvent and the

spin distributions changes little by the solvation effect.

In summary, **2a**, **4a**, and **6a** have essentially the same electronic structure of the doublet state in gas phase and weakly polar solvent except that the orbital mixing between **M** and salen ligand becomes larger when going from the Pd(II) to the Pt(II). In strongly polar solvent, the electronic structures of **2a** and **4a** become localized, leading to the asymmetrical C_1 geometry and significantly different spin population between the $(\text{PhO}+\text{CN})^1$ and $(\text{PhO}+\text{CN})^2$ moieties. However, such localization does not occur in **6a** even in strongly polar solvent.

Vertical $\pi_b \rightarrow d_{xz}$ Excitation from the Ground State of the Re(III) Complexes **5a** and **5b**

To evaluate the $\pi_b \rightarrow d_{xz}$ excitation, we must employ more states in the state averaged GMC-SCF calculation because several $d \rightarrow d$ excitations exist at lower energy than the $\pi_b \rightarrow d_{xz}$ excitation. For such investigation, we employed the nine-state averaged GMC-QDPT(SAS2/SAS2) method for the ground state, the lowest energy four $d \rightarrow d$ excited states, the lowest energy two $\pi \rightarrow d_{yz}$ excited states, and the lowest energy two $\pi \rightarrow d_{xz}$ excited states, which is called "9SA-GMC-QDPT(SAS2/SAS2)"; see Refs. [48] and [50] in main text for details of the SAS2 and parent determinants. The 9SA-GMC-QDPT(SAS2/SAS2)-calculated excitation energies ΔE , oscillator strengths f , and dipole moments μ_x are shown in Table S20 in ESI.

The 9SA-GMC-QDPT(SAS2/SAS2)-calculated excitation energies to the $d_{z^2} \rightarrow d_{yz}$, $\pi_b \rightarrow d_{yz}$, and $\pi_a \rightarrow d_{yz}$ excited states agree well with those calculated by the 4SA-GMC-QDPT(SAS2/SAS2). The $\pi_b \rightarrow d_{xz}$ excitation exists at higher energy than the $\pi_b \rightarrow d_{yz}$ by about 1.0 eV and the $\pi_a \rightarrow d_{yz}$ excitations by about 0.5 eV but it exhibits much larger oscillator strength than that of the allowed $\pi_a \rightarrow d_{yz}$ excitation, as suggested by the U-TDDFT calculations with the M06 functional. Based on these results, it can be predicted that the allowed $\pi_b \rightarrow d_{xz}$ excitation, which exhibits the LMCT character, is experimentally observed as the largest absorption spectra of **5a** and **5b** in the low energy region. This means that the observation of the $\pi_a \rightarrow d_{yz}$ excitation is not easy because of the small oscillator strength, though it exists at lower energy than the $\pi_b \rightarrow d_{xz}$ one.

Spin Distribution in Quartet State of One-electron Oxidized Salen Complexes of Group 7 Metals

The spin population on the salen ligand changes in a somewhat complicated manner at the U-DFT level in comparison to the charge on the salen ligand, as shown in Tables S21-S22 in ESI, when going from **1a** to **5a** in the quartet state, as follows: The sum of the spin populations on the (PhO+CN)¹ and (PhO+CN)² moieties considerably decreases unlike in the group 10 analogues; it is 0.75 - 0.81 *e* in **1a** depending on solvent but considerably small (-0.15 ~ -0.12 *e*) in **5a**. In **1a** and **3a**, the spin population is mainly localized on the (PhO+CN)² moiety but in **5a** delocalized on the (PhO+CN)¹ and (PhO+CN)² moieties, as shown in Figure S7 in ESI. The spin population of the (PhO+CN)² moiety gradually decreases when going from **1a** to **5a** but that of the (PhO+CN)¹ moiety becomes the most negative in **3a** and then moderately less negative in **5a**, as shown in Table S21. Another important result is that the spin population of the **M** *d*_{xz} orbital becomes much less negative by about 0.5 *e* when going from **1a** to **5a**, while those of other **M** *d* orbitals become moderately less negative by about 0.1 - 0.2 *e*; the former decreases from -0.80 *e* to -0.34 *e* in gas phase and from -0.83 *e* to -0.32 *e* in H₂O. Because the characteristic changes in gas phase are essentially the same as those in solvents, we wish to focus on the spin populations and charges in gas phase for below discussion.

To elucidate the reason why the spin populations on the salen ligand change in a somewhat complicated manner, we performed the NBO analysis, assuming the C₂-symmetry for comparison; see values in parentheses in Tables S21-S23 in ESI for the total spin populations, charges, and α - and β -spin populations. When going from **1a** to **3a** under the C₂-symmetry, the sum of the spin populations on the (PhO+CN)¹ and (PhO+CN)² moieties decreases from 0.75 *e* to 0.21 *e* by 0.54 *e* and the sum of their charges becomes moderately more positive by only 0.06 *e* (Tables S21 and S22), indicating that the α -spin population decreases on the salen ligand by 0.30 *e* but the β -spin population increases by 0.24 *e*. These changes are essentially the same as those in the C₁ symmetry. The α -spin population mainly increases from 0.17 *e* to 0.30 *e* by 0.13 *e* on the **M** *d*_{xz} orbital when going from **1a** to **3a**, as shown in Table S23 in ESI. This is reasonable because the

M d orbitals can more mix with the π orbitals of the salen ligand in **3a** than in **1a**; remember that the **M** 4d forms the larger overlap with the salen O and N atoms than the 3d because of the larger sized of 4d than that of 3d. In other words, the main configuration is represented by $(\pi_a + \delta d_{xz})^\alpha (d_{xz} - \delta \pi_a)^\beta (d_{yz})^\beta (d_{z^2})^\beta (d_{x^2-y^2})^\beta$ ($\delta \ll 1$) in the spin-restricted picture and the LCAO coefficient δ becomes larger in **3a** than in **1a**.^{S7} As a result, when going from **1a** to **3a**, the α -spin population decreases on the salen ligand, increases on the **M**, and the **M**-O and **M**-N bond orders increase in the α -spin space, as shown in Table S18B in ESI. Because the orbital mixing is larger in **3a** than in **1a**, the β -spin LUMO ($\pi_a - \delta d_{xz}$) exists at higher energy in **3a** than in **1a** by 0.21 eV, as shown in Figure S8, which has a hole produced by one-electron oxidation. This feature indicates that the orbital mixing of the **M** d_{xz} orbital with the salen π_a orbital is larger in the β -spin LUMO of **3a** than in that of **1a** and the β -spin population increases on the salen ligand but decreases by 0.09 e in the **M** d_{xz} and by 0.13 e in the **M** d_{xy} (Table S23).

When going from the C_2 -symmetrical geometry to the asymmetrical C_1 , the orbital mixing between the π_a and π_b orbitals provides the localized π_1 and π_2 orbitals and hence the charge and spin polarizations largely change in both of **1a** and **3a**; the spin population on the (PhO+CN)² moiety increases by about 0.4 e in gas phase and about 0.5 e in H₂O solution and that on the (PhO+CN)¹ moiety decreases by about 0.4 e in gas phase and about 0.5 e in H₂O solution.

When going from **3a** to **5a** under the C_2 -symmetry, the sum of the spin populations on the (PhO+CN)¹ and (PhO+CN)² moieties decreases from 0.21 e to -0.15 e by 0.36 e and the sum of their charges becomes more negative by 0.18 e , indicating that the α -spin population moderately decreases on the salen ligand by 0.09 e but the β -spin population largely increases by 0.27 e . The α -spin population does not increase so much on all the **M** d orbitals (0.31 e on the **M** d_{xz}) but the β -spin population largely decreases from 0.89 e to 0.65 e by 0.24 e on the **M** d_{xz} , as shown in Table S23 in ESI, indicating that the orbital mixing of the salen π_a with the **M** d_{xz} in the β -spin SOMO becomes larger in **5a** to increase the β -spin population on the salen ligand than in **1a** and **3a**. The spin population on the Re d_{xz} (0.31 e in α -spin and 0.65 e in β -spin) also indicates that the α - and β -spin electrons occupy the $(a_1 \pi_a + b_1 d_{xz})$ and $(a_2 d_{xz} + b_2 \pi_a)$ MOs, respectively, in the spin

unrestricted picture, where $a_1 \geq b_1$ and $a_2 \geq b_2$.^{S9} Because of the larger orbital mixing, the β -spin LUMO ($a_2\pi_a - b_2d_{xz}$) of **5a** exists at higher energy than those of **3a** and **1a** by 0.33 and 0.54 eV, respectively, as shown in Figure S8.^{S8} This large orbital mixing of **5a** enhances the **M-O** and **M-N** bond orders, to which the β -spin MO contributes, as shown in Table S18B in ESI.

In summary, the orbital mixing is small in **1a** and **3a**, in which the α - and β -spin SOMOs do not change very much from the salen π_a and **M** d_{xz} orbitals, respectively.^{S10} In **5a**, the orbital mixing is large and the α - and β -spin electrons occupy the $a_1\pi_a + b_1d_{xz}$ and $b_2\pi_a + a_2d_{xz}$ MOs, respectively, in the spin unrestricted picture, where $a_1 \geq b_1$ and $a_2 \geq b_2$. However, the large difference in LCAO coefficients between the $a_1\pi_a + b_1d_{xz}$ and $b_2\pi_a + a_2d_{xz}$ MOs is not consistent with the spin restricted picture. This unreasonable feature suggests that the main configuration $(a\pi_a + bd_{xz})^2(d_{yz})^\beta(d_{z^2})^\beta(d_{x^2-y^2})^\beta$ largely undergoes the mixing of $(a\pi_a + bd_{xz})^\alpha(ad_{xz} - b\pi_a)^\beta(d_{yz})^\beta(d_{z^2})^\beta(d_{x^2-y^2})^\beta$ in the spin restricted picture and hence the **M** d_{xz} has moderate β -spin population in **5a** unlike the large β -spin one in **1a** and **3a**; see Ref. [S9] for details. This large orbital mixing is also the origin of geometry of C_2 -symmetry which does not have mixed-valence nature.

[S7]: In the spin restricted picture, the quartet state is represented by a single reference wave function $(\pi_a + \delta d_{xz})^2(d_{yz})^\beta(d_{z^2})^\beta(d_{x^2-y^2})^\beta$ (named ${}^4\Psi_G$) and its excited state with the quartet spin multiplicity is represented by $(\pi_a + \delta d_{xz})^\alpha(d_{xz} - \delta\pi_a)^\beta(d_{yz})^\beta(d_{z^2})^\beta(d_{x^2-y^2})^\beta$ (named ${}^4\Psi_E$). In the U-DFT calculation, however, the wave function of quartet state was represented by $(\pi_a + \delta d_{xz})^\alpha(d_{xz} + \delta\pi_a)^\beta(d_{yz})^\beta(d_{z^2})^\beta(d_{x^2-y^2})^\beta$. This means that the configuration mixing between ${}^4\Psi_G$ and ${}^4\Psi_E$ is considerably large, suggesting that the multi-reference wave function theory is necessary for correctly understanding the electronic configuration of **1** and **3**. In the quartet ground state, the weight of ${}^4\Psi_G$ is about 10 % even in **3** at the 3SA-GMC-SCF(SAS/SAS) level, while it is about 50 % in the lowest energy quartet state of **5**, indicating that the configuration mixing is not so crucial in **1** and **3** unlike in **5**.

[S8]: On the other hand, the α -spin unoccupied MOs of **5a** such as the **M** d_{xz} and d_{yz} orbitals

exist at the similar energy to those of **3a**, as shown in Figure S4 in ESI, indicating that the orbital mixing between the **M** d orbitals and the salen orbitals does not largely differ in the α -spin space between **5a** and **3a** and hence the α -spin populations on **M** and the salen ligand change little when going from **3a** to **5a**.

[S9]: As shown in Table S23 in ESI, the α - and β -spin populations on the Re d_{xz} are calculated to be 0.31 e and 0.65 e , respectively, at the U-DFT/M06 level, indicating that the β -spin electron does not occupy the $a_2\pi_a + b_2d_{xz}$ but the $b_2\pi_a + a_2d_{xz}$, while the α -spin electron occupies the $a_1\pi_a + b_1d_{xz}$, where the LCAO coefficients are $a_1 \geq b_2$ and $a_2 \geq b_2$). Strictly speaking, the β -spin electron should occupy the $a_2\pi_a + b_2d_{xz}$ even at the U-DFT level because of the similarity between the α - and β -spin MOs and hence the above-mentioned electron configuration is not consistent with the spin restricted picture that the α - and β -spin MOs are the same to each other. This discrepancy arises from the limitation of the single-reference wave function theory, indicating that the lowest energy quartet state of **5** undergoes the large configuration mixing between the $(a\pi_a + b d_{xz})^2 (d_{yz})^\beta (d_{z^2})^\beta (d_{x^2-y^2})^\beta$ and $(a\pi_a + b d_{xz})^\alpha (a d_{xz} - b\pi_a)^\beta (d_{yz})^\beta (d_{z^2})^\beta (d_{x^2-y^2})^\beta$ and hence the multi-reference wave function theory is necessary for correctly understanding in the quartet state of **5** like those of **1** and **3**. As mentioned in Ref. [S7] in ESI, the weight of ${}^4\Psi_G$ (about 50 %) was significantly large in the lowest energy quartet state of **5** at the 3SA-GMC-SCF(SAS/SAS) level. Therefore, we performed the successive QDPT(SAS/SAS) calculation of the lowest energy quartet state of **5**, as was discussed in pages S7-S10 in ESI.

[S10]: Strictly speaking, the α -spin orbital mixing is somewhat larger in **3a** at the U-DFT/M06 level than in **5a**.

Table S1: TDDFT-calculated vertical excitation energy, ΔE , and oscillator strength, f , of one-electron oxidized salen complexes of group 10 metals (Ni(II), Pd(II), and Pt(II)) with substituents (R^1, R^2)=(Me, Me) in the doublet state.^a

functional	ΔE [eV]	f [au]	ΔE [eV]	f [au]	ΔE [eV]	f [au]
	Ni 2a		Pd 4a		Pt 6a	
	in gas phase ^b					
B3LYP	0.774	0.164	0.688	0.157	0.802	0.167
B3PW91	0.775	0.160	0.687	0.159	0.805	0.169
PBE0	0.730	0.179	0.640	0.166	0.620	0.227
CAM-B3LYP	0.710	0.322	0.606	0.306	0.799	0.312
M06-L	0.836	0.100	0.810	0.150	0.891	0.148
M06	0.664	0.161	0.583	0.150	0.705	0.169
M06-2X	0.725	0.411	0.644	0.366	0.794	0.360
LC-BLYP	0.279	0.132	0.141	0.076	0.536	0.210
LC-wPBE	0.421	0.171	0.235	0.117	0.620	0.227
	in CH ₂ Cl ₂ solution ^c					
B3LYP	0.693	0.203	0.613	0.183	0.754	0.212
B3PW91	0.698	0.199	0.614	0.184	0.756	0.215
PBE0	0.637	0.224	0.596	0.173	0.716	0.232
CAM-B3LYP	-0.210	-0.260	1.309	0.111	0.381	0.278
M06-L	0.767	0.111	0.737	0.175	0.853	0.189
M06	0.565	0.204	0.575	0.145	0.643	0.216
M06-2X	-0.070	-0.247	1.229	0.086	0.376	0.280
LC-BLYP	-0.912	-0.284	2.782	0.104	-0.703	-0.311
LC-wPBE	-0.799	-0.272	2.586	0.094	-0.551	-0.301
expt.	0.620		0.508		0.676	

^aCalculated for the lowest energy allowed excitation at the U-TDDFT level; the first excited state is the allowed transition in **2**, **4**, and **6**.

^bGeometry was optimized by the U-DFT with M06 functional.

^cGeometry was optimized by the PCM-U-DFT with M06 functional.

Table S2: TDDFT-calculated vertical excitation energy, ΔE , and oscillator strength, f , of one-electron oxidized salen complexes of group 7 metals (Mn(III), Tc(III), and Re(III)) with substituents (R^1, R^2)=(Me, Me) in the quartet state. ^a

functional	ΔE [eV]	f [au]	ΔE [eV]	f [au]	ΔE [eV]	f [au]
	Mn 1a		Tc 3a		Re 5a	
	in gas phase ^b					
B3LYP	0.497	0.081	0.542	0.060	(1.002 ^c)	(0.042)
B3PW91	0.504	0.086	0.557	0.074	(1.029)	(0.091)
PBE0	0.482	0.086	0.541	0.087	(1.037)	(0.138)
CAM-B3LYP	1.252	0.045	1.172	0.066	(1.077)	(0.147)
M06-L	0.569	0.055	0.587	0.023	(1.045)	(0.019)
M06	0.446	0.062	0.509	0.036	(1.026)	(0.064)
M06-2X	1.042	0.046	0.979	0.092	(0.973)	(0.220)
LC-BLYP	2.768	0.031	2.500	0.060	(1.194)	(0.179)
LC-wPBE	2.613	0.032	2.338	0.061	(1.101)	(0.204)
	in CH ₂ Cl ₂ solution ^d					
B3LYP	0.583	0.067	0.653	0.144	(1.268)	(0.076)
B3PW91	0.594	0.068	0.657	0.155	(1.239)	(0.103)
PBE0	0.751	0.054	0.694	0.150	(1.240)	(0.121)
CAM-B3LYP	1.986	0.027	1.389	0.104	(1.458)	(0.053)
M06-L	0.563	0.099	0.723	0.121	(1.173)	(0.086)
M06	0.804	0.042	0.702	0.125	(1.211)	(0.061)
M06-2X	1.825	0.019	1.380	0.095	(1.753)	(0.113)
LC-BLYP	3.576	0.046	2.890	0.209	(2.143)	(0.124)
LC-wPBE	3.426	0.017	2.702	0.166	(1.974)	(0.139)
expt.	0.838		-		-	

^aCalculated for the lowest energy allowed excitation at the U-TDDFT level; the first excited state is the allowed transition in **1** and **3** but the forbidden transition in **5**.

^bGeometry was optimized by the U-DFT with M06 functional.

^cIn parentheses are not the excitation from the ground state, because the ground state is not quartet but doublet in **5**.

^dGeometry was optimized by the PCM-U-DFT with M06 functional.

Table S3: Important geometrical parameters, x -component of dipole moment μ_x , and relative free energy ΔA , of non-oxidized metal-salen complexes in CH_2Cl_2 .^a

M	spin	geom.	L/D ^b	Bond length ^c [Å]						μ_x ^d	ΔA ^e	
				C-O ¹	C-O ²	M-O ¹	M-O ²	M-N ¹	M-N ²			
Group 10 metal												
Ni	2ⁿa	1et ^f	C ₂	D	1.29	1.29	1.85	1.85	1.85	1.85	0.00	-
Pd	4ⁿa	1et ^f	C ₂	D	1.30	1.30	2.02	2.02	1.98	1.98	0.00	-
Pt	6ⁿa	1et ^f	C ₂	D	1.30	1.30	2.02	2.02	1.97	1.97	0.00	-
Group 7 metal												
Mn	1ⁿa	1et ^f	C ₂	D	1.32	1.32	1.71	1.71	1.97	1.97	0.00	74.6
		3et	C ₁	L	1.30	1.28	1.85	1.89	1.92	1.92	6.59	30.8
		5et	C ₂	D	1.32	1.32	1.84	1.84	1.95	1.95	0.00	0.0
Tc	3ⁿa	1et ^f	C ₂ -like	D	1.32	1.32	1.87	1.87	2.08	2.08	0.02	11.7
		3et	C ₂ -like	D	1.31	1.31	1.96	1.97	2.03	2.03	0.22	8.2
		5et	C ₂ -like	D	1.32	1.32	1.98	1.98	2.06	2.06	0.01	0.0
Re	5ⁿa	1et ^f	C ₂	D	1.33	1.33	1.82	1.82	2.04	2.04	0.00	0.0
		3et	C ₂	D	1.34	1.34	1.89	1.89	2.03	2.03	0.00	1.7
		5et	C ₂	D	1.33	1.33	1.97	1.97	2.03	2.03	0.00	7.7

^aCalculated by the U-DFT and 3D-RISM-SCF-U-DFT with M06 functional.

^b"L" and "D" represent the localized and delocalized electronic state, respectively.

^cSee Scheme 2a for O¹ and O² atoms.

^dUnit is in [Debye].

^eUnit is in [kcal mol⁻¹]

^fThe singlet state was evaluated by the 3D-RISM-SCF-R-DFT with M06 functional.

Table S4: Main electron configurations of non-oxidized metal-salen complexes in CH_2Cl_2 .^{a,b,c}

M		spin	geom.	M				Salen ligand	
Group 7 metal									
				$d_{xz}(+\delta\pi_a)$	$d_{yz}(+\delta\pi_b)$	d_{z^2}	$d_{x^2-y^2}$	$\pi_b(-\delta d_{yz})$	$\pi_a(-\delta d_{xz})$
Mn	1ⁿa	1et ^d	C_2	0	2	2	0	2	2
Tc	3ⁿa	1et ^d	C_2 -like	0	2	2	0	2	2
Re	5ⁿa	1et ^d	C_2	0	2	2	0	2	2
Mn	1ⁿa	3et	C_1	β	2	β	β	2	α
Tc	3ⁿa	3et	C_2 -like	0	2	β	β	2	2
Re	5ⁿa	3et	C_2	0	β	2	β	2	2
Mn	1ⁿa	5et	C_2	β	β	β	β	2	2
Tc	3ⁿa	5et	C_2 -like	β	β	β	β	2	2
Re	5ⁿa	5et	C_2	β	β	β	β	2	2
Group 10 metal									
				$d_{xz}(+\delta\pi_a)$	$d_{yz}(+\delta\pi_b)$	d_{z^2}	$d_{x^2-y^2}$	$\pi_b(-\delta d_{yz})$	$\pi_a(-\delta d_{xz})$
Ni	2ⁿa	1et ^d	C_2	2	2	2	2	2	2
Pd	4ⁿa	1et ^d	C_2	2	2	2	2	2	2
Pt	6ⁿa	1et ^d	C_2	2	2	2	2	2	2

^aCalculated by the U-DFT and 3D-RISM-SCF-U-DFT with M06 functional.

^b" α ", " β ", "2", "0" represent α - and β -spin SOMOs, DOMO, and unoccupied MO, respectively.

^cIn case of the C_1 -symmetrical geometry, π_b and π_a change to π_1 and π_2 , respectively.

^dThe singlet state was evaluated by the 3D-RISM-SCF-R-DFT with M06 functional.

Table S5: (A) NBO spin populations and (B) charges of non-oxidized salen complexes of group 7 metals in the quintet state in CH₂Cl₂.^{a,b}

M		M						Salen ligand ^c		
		(A) Spin population								
		<i>nd_{xz}</i>	<i>nd_{yz}</i>	<i>nd_{z²}</i>	<i>nd_{x²-y²}</i>	<i>nd_{xy}</i>	(<i>n</i> + 1)s	sides-1+2	side-1	side-2
Mn	1ⁿa	-0.818	-0.892	-0.928	-0.874	-0.226	-0.053	-0.202	-0.101	-0.101
Tc	3ⁿa	-0.736	-0.824	-0.857	-0.816	-0.091	-0.108	-0.532	-0.276	-0.276
Re	5ⁿa	-0.746	-0.783	-0.814	-0.814	-0.061	-0.175	-0.584	-0.292	-0.292
		(B) Charge								
		charge	population					charge		
	M	<i>nd_{xz}</i>	<i>nd_{yz}</i>	<i>nd_{z²}</i>	<i>nd_{x²-y²}</i>	<i>nd_{xy}</i>	(<i>n</i> + 1)s	sides-1+2	side-1	side-2
Mn	1ⁿa	1.554	1.157	1.064	1.038	1.099	0.803	0.250	-1.212	-0.606
Tc	3ⁿa	1.500	1.233	1.083	1.032	1.143	0.711	0.277	-1.160	-0.580
Re	5ⁿa	1.600	1.191	1.038	0.965	1.113	0.660	0.402	-1.266	-0.633

^aCalculated by the U-DFT and 3D-RISM-SCF-U-DFT the M06 functional.

^bSide-1 and 2 represent (PhO+CN)¹ and (PhO+CN)² moieties, respectively; see Scheme 2a for (PhO+CN)¹ and (PhO+CN)² moieties.

^cThe spin populations and charges on the (PhO+CN)¹ and (PhO+CN)² moieties are calculated as the sum of their site-components, respectively.

Table S6: Important geometrical parameters, x -component of dipole moment μ_x , and difference in RISM (Helmholtz) free energy $\Delta A_{C_1-C_2}$ between the C_1 - and C_2 -symmetrical geometries of one-electron oxidized salen complexes of group 10 metals in the doublet state.^a

M	solvent	geom.	L/D ^b	Bond length ^c [Å]						μ_x ^d	$\Delta A_{C_1-C_2}$ ^e	
				C-O ¹	C-O ²	M-O ¹	M-O ²	M-N ¹	M-N ²			
Ni	2a	none	C_2	D	1.28	1.28	1.83	1.83	1.84	1.84	0.00	-0.0
		CH ₂ Cl ₂	C_2 -like	D	1.28	1.28	1.84	1.84	1.85	1.85	0.03	-0.1
		CH ₃ OH	C_2 -like	D	1.28	1.28	1.84	1.84	1.85	1.85	0.12	-0.2
		H ₂ O	C_1	L	1.30	1.27	1.84	1.87	1.84	1.85	9.33	-0.3
	2b	none	C_2	D	1.28	1.28	1.84	1.84	1.85	1.85	0.00	-0.0
		CH ₂ Cl ₂	C_2	D	1.28	1.28	1.84	1.84	1.85	1.85	0.00	-0.1
		CH ₃ OH	C_1	L	1.30	1.27	1.82	1.86	1.84	1.85	7.29	-0.3
		H ₂ O	C_1	L	1.31	1.27	1.84	1.88	1.84	1.86	11.90	-0.7
	2c	none	C_1	L	1.29	1.27	1.82	1.85	1.84	1.86	9.21	
		CH ₂ Cl ₂	C_1	L	1.29	1.27	1.82	1.87	1.84	1.87	14.17	
		CH ₃ OH	C_1	L	1.30	1.27	1.82	1.87	1.84	1.87	15.73	
		H ₂ O	C_1	L	1.30	1.27	1.83	1.87	1.84	1.86	17.11	
Pd	4a	none	C_2 -like	D	1.28	1.28	2.01	2.01	1.97	1.97	0.01	-0.0
		CH ₂ Cl ₂	C_2 -like	D	1.28	1.28	2.01	2.01	1.97	1.97	0.31	-0.3
		CH ₃ OH	C_1	L	1.30	1.27	2.00	2.03	1.96	1.98	7.47	-0.5
		H ₂ O	C_1	L	1.31	1.27	2.00	2.05	1.96	1.98	10.78	-1.2
	4b	none	C_2 -like	D	1.28	1.28	2.01	2.01	1.97	1.97	0.01	-0.0
		CH ₂ Cl ₂	C_2 -like	D	1.28	1.28	2.01	2.01	1.97	1.97	0.03	-0.3
		CH ₃ OH	C_1	L	1.30	1.27	2.00	2.04	1.96	1.98	10.22	-0.7
		H ₂ O	C_1	L	1.31	1.27	2.00	2.05	1.96	1.98	12.85	-1.6
	4c	none	C_1	L	1.29	1.27	1.99	2.03	1.96	1.99	10.23	
		CH ₂ Cl ₂	C_1	L	1.30	1.27	1.99	2.04	1.96	1.99	15.10	
		CH ₃ OH	C_1	L	1.30	1.27	2.00	2.04	1.96	1.99	16.68	
		H ₂ O	C_1	L	1.30	1.27	2.00	2.04	1.96	1.99	17.81	
Pt	6a	none	C_2	D	1.29	1.29	1.99	1.99	1.95	1.95	0.00	-0.0
		CH ₂ Cl ₂	C_2 -like	D	1.29	1.29	1.99	1.99	1.95	1.95	0.03	-0.0
		CH ₃ OH	C_2 -like	D	1.30	1.30	1.99	1.99	1.95	1.95	0.06	-0.0
		H ₂ O	C_2 -like	D	1.30	1.30	1.99	1.99	1.95	1.95	0.09	-0.0
	6b	none	C_2	D	1.29	1.29	1.99	1.99	1.95	1.95	0.00	-0.0
		CH ₂ Cl ₂	C_2 -like	D	1.29	1.29	2.00	2.00	1.95	1.95	0.01	-0.0
		CH ₃ OH	C_2 -like	D	1.30	1.30	2.00	2.00	1.95	1.95	0.03	-0.0
		H ₂ O	C_2 -like	D	1.30	1.30	2.00	2.00	1.95	1.95	0.42	-0.0
	6c	none	C_1	L	1.30	1.28	1.99	2.00	1.95	1.96	7.90	
		CH ₂ Cl ₂	C_1	L	1.30	1.28	1.99	2.01	1.95	1.96	11.80	
		CH ₃ OH	C_1	L	1.31	1.28	1.99	2.01	1.95	1.96	13.61	
		H ₂ O	C_1	L	1.31	1.28	2.00	2.02	1.95	1.96	15.22	

^aCalculated by the U-DFT and 3D-RISM-SCF-U-DFT with M06 functional.

^b"L" and "D" represent the localized and delocalized electronic state, respectively.

^cSee Scheme 2a for O¹ and O² atoms.

^dUnit is in [Debye].

^eUnit is in [kcal mol⁻¹]

Table S7: Important geometrical parameters, x -component of dipole moment μ_x , and difference in RISM (Helmholtz) free energy $\Delta A_{C_1-C_2}$ between the C_1 - and C_2 -symmetrical geometries of one-electron oxidized salen complexes of group 7 metals in the quartet state.^a

M	solvent	geom.	L/D ^b	Bond length ^c [Å]						μ_x ^d	$\Delta A_{C_1-C_2}$ ^e	
				C-O ¹	C-O ²	M-O ¹	M-O ²	M-N ¹	M-N ²			
Mn	1a	none	C_1	L	1.32	1.27	1.80	1.90	1.92	1.98	6.13	-0.2
		CH ₂ Cl ₂	C_1	L	1.32	1.27	1.80	1.91	1.93	1.98	9.06	-1.2
		CH ₃ OH	C_1	L	1.32	1.27	1.81	1.91	1.92	1.98	10.70	-2.0
		H ₂ O	C_1	L	1.32	1.27	1.82	1.92	1.93	1.98	11.59	-2.5
	1b	none	C_2 -like	D	1.30	1.30	1.84	1.84	1.95	1.95	0.48	-0.0
		CH ₂ Cl ₂	C_1	L	1.32	1.28	1.81	1.90	1.92	1.98	10.53	-1.0
		CH ₃ OH	C_1	L	1.32	1.27	1.82	1.91	1.95	1.99	12.72	-1.8
		H ₂ O	C_1	L	1.32	1.28	1.82	1.91	1.93	1.98	13.82	-2.6
	1c	none	C_1	L	1.32	1.28	1.80	1.90	1.92	1.99	12.79	
		CH ₂ Cl ₂	C_1	L	1.32	1.28	1.81	1.90	1.93	1.98	15.74	
		CH ₃ OH	C_1	L	1.32	1.28	1.81	1.89	1.93	1.98	17.26	
		H ₂ O	C_1	L	1.32	1.28	1.82	1.89	1.93	1.97	18.19	
Tc	3a	none	C_1	L	1.31	1.29	1.95	2.00	2.03	2.06	3.76	-0.2
		CH ₂ Cl ₂	C_1	L	1.32	1.28	1.95	2.00	2.03	2.06	5.50	-0.4
		CH ₃ OH	C_1	L	1.32	1.28	1.95	2.00	2.02	2.07	7.18	-0.6
		H ₂ O	C_1	L	1.32	1.28	1.95	2.01	2.03	2.06	8.29	-0.9
	3b	none	C_2 -like	D	1.30	1.30	1.97	1.97	2.04	2.04	0.20	-0.0
		CH ₂ Cl ₂	C_1	L	1.31	1.28	1.95	2.01	2.03	2.06	7.06	-0.6
		CH ₃ OH	C_1	L	1.32	1.28	1.95	2.01	2.03	2.07	9.39	-0.9
		H ₂ O	C_1	L	1.32	1.28	1.95	2.01	2.03	2.06	10.91	-1.3
	3c	none	C_1	L	1.32	1.28	1.94	2.02	2.04	2.08	11.27	
		CH ₂ Cl ₂	C_1	L	1.32	1.28	1.95	2.02	2.04	2.08	14.33	
		CH ₃ OH	C_1	L	1.32	1.28	1.95	2.02	2.04	2.07	16.05	
		H ₂ O	C_1	L	1.32	1.28	1.96	2.02	2.04	2.07	17.10	
Re	5a	none	C_2	D	1.32	1.32	1.92	1.92	2.00	2.00	0.00	-0.0
		CH ₂ Cl ₂	C_2	D	1.32	1.32	1.92	1.92	2.00	2.00	0.00	-0.0
		CH ₃ OH	C_2 -like	D	1.32	1.32	1.92	1.92	2.00	2.00	0.01	-0.0
		H ₂ O	C_2 -like	D	1.32	1.32	1.92	1.92	2.00	2.00	0.02	-0.1
	5b	none	C_2	D	1.32	1.32	1.92	1.92	2.01	2.01	0.00	-0.0
		CH ₂ Cl ₂	C_2 -like	D	1.31	1.31	1.93	1.93	2.01	2.01	0.08	-0.0
		CH ₃ OH	C_2 -like	D	1.31	1.31	1.92	1.92	2.00	2.00	0.10	-0.0
		H ₂ O	C_2 -like	D	1.32	1.32	1.92	1.92	2.00	2.00	0.11	-0.1
	5c	none	C_1	L	1.33	1.31	1.91	1.93	2.01	2.01	6.51	
		CH ₂ Cl ₂	C_1	L	1.32	1.30	1.92	1.94	2.01	2.02	9.15	
		CH ₃ OH	C_1	L	1.32	1.30	1.93	1.94	2.01	2.02	9.51	
		H ₂ O	C_1	L	1.32	1.30	1.92	1.93	2.00	2.01	9.92	

^aCalculated by the U-DFT and 3D-RISM-SCF-U-DFT with M06 functional.

^b"L" and "D" represent the localized and delocalized electronic state, respectively.

^cSee Scheme 2a for O¹ and O² atoms.

^dUnit is in [Debye].

^eUnit is in [kcal mol⁻¹]

Table S8: Main electron configurations of one-electron oxidized metal-salen complexes in CH_2Cl_2 .^{a,b,c}

M		spin	geom.	M				Salen ligand	
Group 10 metal									
				$d_{xz}(+\delta\pi_a)$	d_{yz}	d_{z^2}	$d_{x^2-y^2}$	π_b	$\pi_a(-\delta d_{xz})$
Ni	2a	2et	C_2 -like	2	2	2	2	2	α
Pd	4a	2et	C_2 -like	2	2	2	2	2	α
Pt	6a	2et	C_2 -like	2	2	2	2	2	α
Group 7 metal									
				$d_{xz}(+\delta\pi_a)$	d_{yz}	d_{z^2}	$d_{x^2-y^2}$	π_b	$\pi_a(-\delta d_{xz})$
Mn	1a	2et	C_2 -like	β	2	β	β	α	α
Tc	3a	2et	C_2 -like	0	2	β	0	2	2
Re	5a	2et	C_2	0	β	2	0	2	2
				$d_{xz}(+\delta\pi_a)$	d_{yz}	d_{z^2}	$d_{x^2-y^2}$	π_b	$\pi_a(-\delta d_{xz})$
Mn	1a	4et	C_1	β	β	β	β	2	α
Tc	3a	4et	C_1	β	β	β	β	2	α
Re	5a	4et	C_2	0	β	β	β	2	2
				$d_{xz}(+\delta\pi_a)$	d_{yz}	d_{z^2}	$d_{x^2-y^2}$	π_b	$\pi_a(-\delta d_{xz})$
Mn	1a	6et	C_1	β	β	β	β	β	2
Tc	3a	6et	C_1	β	β	β	β	β	2
Re	5a	6et	C_1	β	β	β	β	β	2

^aCalculated by the U-DFT and 3D-RISM-SCF-U-DFT with M06 functional.

^b" α ", " β ", "2", "0" represent α - and β -spin SOMOs, DOMO, and unoccupied MO, respectively.

^cIn case of the C_1 -symmetrical geometry, π_b and π_a change to π_1 and π_2 , respectively, except for the sextet state of one-electron oxidized salen complexes of group 7 metals in which π_b and π_a change to π_2 and π_1 , respectively

Table S9: Important geometrical parameters, x -component of dipole moment μ_x , and relative free energy ΔA , of one-electron oxidized metal-salen complexes in the different spin states in CH_2Cl_2 .^a

M	spin	geom.	L/D ^b	Bond length ^c [Å]						μ_x ^d	ΔA ^e	
				C-O ¹	C-O ²	M-O ¹	M-O ²	M-N ¹	M-N ²			
Group 10 metal												
Ni	2a	2et	C ₂ -like	D	1.28	1.28	1.84	1.84	1.85	1.85	0.03	-
Pd	4a	2et	C ₂ -like	D	1.28	1.28	2.01	2.01	1.97	1.97	0.31	-
Pt	6a	2et	C ₂ -like	D	1.29	1.29	1.99	1.99	1.95	1.95	0.05	-
Group 7 metal												
Mn	1a	2et	C ₂ -like	D	1.32	1.32	1.90	1.90	1.93	1.93	0.02	20.0
		4et	C ₁	L	1.32	1.27	1.80	1.91	1.93	1.98	9.06	0.0
		6et	C ₁	L	1.32	1.27	1.80	1.94	1.92	1.99	10.05	3.1
Tc	3a	2et	C ₂ -like	D	1.32	1.32	1.85	1.85	2.09	2.09	0.12	4.9
		4et	C ₁	L	1.32	1.28	1.95	2.00	2.03	2.06	5.50	0.0
		6et	C ₁	L	1.32	1.27	1.95	2.08	2.03	2.08	8.57	6.0
Re	5a	2et	C ₂	D	1.34	1.34	1.80	1.80	2.05	2.05	0.00	0.0
		4et	C ₂	D	1.32	1.32	1.92	1.92	2.03	2.03	0.00	7.1
		6et	C ₁	L	1.33	1.28	1.95	2.06	2.00	2.05	9.96	23.3

^aCalculated by the U-DFT and 3D-RISM-SCF-U-DFT with M06 functional.

^b"L" and "D" represent the localized and delocalized electronic state, respectively.

^cSee Scheme 2a for O¹ and O² atoms.

^dUnit is in [Debye].

^eUnit is in [kcal mol⁻¹]

The Mn(III) and Tc(III) complexes **1a** and **3a** take the asymmetrical (C₁-symmetrical) geometry and exhibit the localized electronic structure in the quartet state, while the Re(III) complex **5a** takes the C₂-symmetrical geometry and exhibits the delocalized electronic structure in the quartet state like in the doublet state, as shown in Table 1B. In the sextet state, all the three complexes **1a**, **3a**, and **5a** take the asymmetrical geometry and exhibit the localized electronic structure.

Table S10: Solvent effect on geometrical symmetry and difference in PCM (Helmholtz) free energy $\Delta A_{C_1-C_2}$ between the C_1 - and C_2 -symmetrical geometries of one-electron oxidized salen complexes of group 10 metals in the doublet state.^a

M	solvent	ϵ^b	geom.	(Me,Me)		(OMe,OMe)			
				L/D ^c	$\Delta A_{C_1-C_2}^d$	geom.	L/D	$\Delta A_{C_1-C_2}$	
Ni	none	-	C_2	D	-0.00	C_2	D	-0.00	
	toluene	2.4	C_2	D	-0.00	C_2	D	-0.00	
	chloro-benzene	5.7	C_2	D	-0.00	C_2	D	-0.00	
	aniline	6.9	C_2	D	-0.00	C_1	L	-0.02	
	CH ₂ Cl ₂	8.9	C_2 -like	D	-0.01	C_1	L	-0.06	
	CH ₃ OH	32.6	C_1	L	-0.06	C_1	L	-0.27	
	H ₂ O	78.4	C_1	L	-0.10	C_1	L	-0.33	
	Pd	none	-	C_2	D	-0.00	C_2	D	-0.00
Pd	toluene	2.4	C_2	D	-0.00	C_2	D	-0.00	
	chloro-benzene	5.7	C_1	L	-0.07	C_1	L	-0.18	
	aniline	6.9	C_1	L	-0.11	C_1	L	-0.27	
	CH ₂ Cl ₂	8.9	C_1	L	-0.18	C_1	L	-0.37	
	CH ₃ OH	32.6	C_1	L	-0.40	C_1	L	-0.69	
	H ₂ O	78.4	C_1	L	-0.47	C_1	L	-0.78	
	Pt	none	-	C_2	D	-0.00	C_2	D	-0.00
		toluene	2.4	C_2	D	-0.00	C_2	D	-0.00
chloro-benzene		5.7	C_2	D	-0.00	C_2	D	-0.00	
aniline		6.9	C_2	D	-0.00	C_2	D	-0.00	
CH ₂ Cl ₂		8.9	C_2	D	-0.00	C_2	D	-0.00	
CH ₃ OH		32.6	C_2	D	-0.00	C_2	D	-0.00	
H ₂ O		78.4	C_2	D	-0.00	C_2	D	-0.00	

^aCalculated by the PCM-U-DFT method with M06 functional.

^bStatic dielectric constant of solvent.

^c"L" and "D" represent the localized and delocalized electronic state, respectively.

^dUnit is in [kcal mol⁻¹].

Table S11: Solvent effect on geometrical symmetry and difference in PCM (Helmholtz) free energy $\Delta A_{C_1-C_2}$ between the C_1 - and C_2 -symmetrical geometries of one-electron oxidized salen complexes of group 7 metals in the quartet state.^a

M	solvent	ϵ^b	geom.	(Me,Me)		(OMe,OMe)		
				L/D ^c	$\Delta A_{C_1-C_2}^d$	geom.	L/D	$\Delta A_{C_1-C_2}$
Mn	none	-	C_1	L	-0.18	C_2 -like	D	-0.03
	toluene	2.4	C_1	L	-1.18	C_1	L	-0.82
	chloro-benzene	5.7	C_1	L	-1.98	C_1	L	-1.79
	aniline	6.9	C_1	L	-2.11	C_1	L	-1.94
	CH ₂ Cl ₂	8.9	C_1	L	-2.25	C_1	L	-2.11
	CH ₃ OH	32.6	C_1	L	-2.80	C_1	L	-2.59
	H ₂ O	78.4	C_1	L	-2.89	C_1	L	-2.71
Tc	none	-	C_1	L	-0.16	C_2 -like	D	-0.01
	toluene	2.4	C_1	L	-0.20	C_1	L	-0.27
	chloro-benzene	5.7	C_1	L	-0.35	C_1	L	-0.57
	aniline	6.9	C_1	L	-0.37	C_1	L	-0.63
	CH ₂ Cl ₂	8.9	C_1	L	-0.40	C_1	L	-0.69
	CH ₃ OH	32.6	C_1	L	-0.47	C_1	L	-0.86
	H ₂ O	78.4	C_1	L	-0.50	C_1	L	-0.90
Re	none	-	C_2	D	-0.00	C_2	D	-0.00
	toluene	2.4	C_2	D	-0.00	C_2	D	-0.00
	chloro-benzene	5.7	C_2	D	-0.00	C_2 -like	D	-0.01
	aniline	6.9	C_2	D	-0.00	C_2 -like	D	-0.01
	CH ₂ Cl ₂	8.9	C_2	D	-0.00	C_2 -like	D	-0.01
	CH ₃ OH	32.6	C_2 -like	D	-0.01	C_2 -like	D	-0.01
	H ₂ O	78.4	C_2 -like	D	-0.01	C_2 -like	D	-0.01

^aCalculated by PCM-U-DFT with M06 functional.

^bStatic dielectric constant of solvent.

^c"L" and "D" represent the localized and delocalized electronic state, respectively.

^dUnit is in [kcal mol⁻¹].

Table S12: (A) NBO spin populations and (B) charges of one-electron oxidized salen complexes of the Re(III) with the (Me, Me) substituents in the doublet state.^{a,b}

		M					Salen ligand ^c				
		(A) Spin population									
		<i>nd_{xz}</i>	<i>nd_{yz}</i>	<i>nd_{z²}</i>	<i>nd_{x²-y²}</i>	<i>nd_{xy}</i>	(<i>n</i> + 1)s	sides-1+2	side-1	side-2	
		Re 5a									
none	C ₂	0.086	0.672	0.039	0.049	0.028	-0.002	0.132	0.066	0.066	
CH ₂ Cl ₂	C ₂	0.084	0.679	0.041	0.050	0.029	0.000	0.122	0.061	0.061	
CH ₃ OH	C ₂ -like	0.087 (0.087 ^d)	0.670 (0.670)	0.062 (0.062)	0.045 (0.045)	0.029 (0.029)	0.001 (0.001)	0.108 (0.108)	0.053 (0.054)	0.055 (0.054)	
H ₂ O	C ₂ -like	0.082 (0.083)	0.667 (0.666)	0.068 (0.068)	0.049 (0.049)	0.029 (0.029)	0.002 (0.002)	0.106 (0.106)	0.052 (0.053)	0.054 (0.053)	
		(B) Charge									
		charge	population					charge			
		M	<i>nd_{xz}</i>	<i>nd_{yz}</i>	<i>nd_{z²}</i>	<i>nd_{x²-y²}</i>	<i>nd_{xy}</i>	(<i>n</i> + 1)s	sides-1+2	side-1	side-2
		Re 5a									
none	C ₂	1.511	0.735	1.118	1.688	0.659	0.706	0.574	-0.336	-0.168	-0.168
CH ₂ Cl ₂	C ₂	1.537	0.723	1.110	1.687	0.661	0.706	0.567	-0.338	-0.169	-0.169
CH ₃ OH	C ₂ -like	1.547 (1.547)	0.721 (0.721)	1.127 (1.127)	1.668 (1.668)	0.651 (0.651)	0.708 (0.708)	0.569 (0.569)	-0.340 (-0.340)	-0.171 (-0.170)	-0.169 (-0.170)
H ₂ O	C ₂ -like	1.767 (1.767)	0.713 (0.713)	1.126 (1.126)	1.664 (1.664)	0.657 (0.657)	0.707 (0.707)	0.560 (0.560)	-0.352 (-0.352)	-0.177 (-0.176)	-0.175 (-0.176)

^aCalculated by the U-DFT and 3D-RISM-SCF-U-DFT the M06 functional.

^bSide-1 and 2 represent (PhO+CN)¹ and (PhO+CN)² moieties, respectively; see Scheme 2a for (PhO+CN)¹ and (PhO+CN)² moieties.

^cThe spin populations and charges on the (PhO+CN)¹ and (PhO+CN)² moieties are calculated as the sum of their site-components, respectively.

^dIn parentheses are calculated at the C₂-symmetrical geometry.

Table S13: 2SA-GMC-QDPT(SAS/SAS)-calculated vertical excitation energy ΔE , oscillator strength f , and dipole moment μ_x^0 and μ_x^{ex} in the $\pi \rightarrow \pi$ excitation of one-electron oxidized salen complexes of (A) group 10 metals with the doublet state and (B) group 7 analogues with the quartet state.^{a,b}

solvent	(Me,Me)			(OMe,OMe)			(Cl,OMe)		
	ΔE [eV]	f [au]	$\mu_x^{\text{ex}}/\mu_x^{\text{gr}}$ [Debye]	ΔE [eV]	f [au]	$\mu_x^{\text{ex}}/\mu_x^{\text{gr}}$ [Debye]	ΔE [eV]	f [au]	$\mu_x^{\text{ex}}/\mu_x^{\text{gr}}$ [Debye]
(A) Group 10 metal									
		Ni(II) 2a			Ni(II) 2b			Ni(II) 2c	
none	0.479	0.404	0.0/0.0	0.460	0.401	0.0/0.0	0.812	0.242	-8.9/15.6
CH ₂ Cl ₂	0.492	0.414	0.0/0.0	0.454	0.394	0.0/0.0	1.465	0.138	-9.4/19.0
CH ₃ OH	0.511	0.397	-3.8/3.9	0.905	0.216	-11.9/13.8	1.628	0.093	-8.4/19.0
H ₂ O	1.230	0.164	-12.7/14.8	1.426	0.124	-12.6/16.3	1.807	0.092	-7.9/20.6
Expt. ^c	0.620 (0.583)			0.579			0.885		
		Pd(II) 4a			Pd(II) 4b			Pd(II) 4c	
none	0.330	0.304	0.0/0.0	0.402	0.379	0.0/0.0	0.827	0.185	-10.6/16.8
CH ₂ Cl ₂	0.414	0.378	-1.0/1.0	0.393	0.367	-0.1/0.1	1.466	0.106	-10.1/19.9
CH ₃ OH	0.871	0.178	-13.0/14.4	1.102	0.130	-13.3/16.1	1.633	0.093	-9.4/20.7
H ₂ O	1.333	0.113	-13.5/16.1	1.522	0.099	-12.9/17.3	1.823	0.070	-8.2/21.4
Expt. ^c	0.508 (0.508)								
		Pt(II) 6a			Pt(II) 6b			Pt(II) 6c	
none	0.642	0.530	0.0/0.0	0.598	0.517	0.0/0.0	0.901	0.461	-5.9/12.9
CH ₂ Cl ₂	0.644	0.529	-0.1/0.1	0.603	0.518	-0.1/0.1	1.188	0.383	-6.5/16.6
CH ₃ OH	0.649	0.529	-0.1/0.1	0.604	0.517	-0.1/0.1	1.367	0.351	-6.3/17.9
H ₂ O	0.659	0.524	-0.1/0.1	0.605	0.512	-0.9/1.1	1.538	0.318	-5.4/18.9
Expt. ^c	0.676 (0.676)								
(B) Group 7 metal									
		Mn 1a			Mn 1b			Mn 1c	
none	0.730	0.168	-16.4/12.8	0.346	0.383	-2.3/2.2	1.314	0.061	-14.2/19.1
CH ₂ Cl ₂	1.113	0.103	-16.7/14.6	1.126	0.117	-16.4/16.0	1.699	0.042	-12.0/20.8
CH ₃ OH	1.380	0.080	-15.4/15.5	1.493	0.079	-15.8/17.7	1.838	0.040	-10.2/21.8
H ₂ O	1.433	0.069	-14.3/16.0	1.658	0.078	-14.8/18.2	2.012	0.038	-9.0/22.3
Expt. ^c	0.838			0.976			1.389		
		Tc 3a			Tc 3b			Tc 3c	
none	0.579	0.278	-13.7/11.4	0.415	0.508	-1.7/1.5	1.130	0.095	-14.0/19.5
CH ₂ Cl ₂	0.700	0.203	-14.8/13.7	0.773	0.178	-15.5/15.4	1.440	0.070	-12.2/21.0
CH ₃ OH	0.907	0.147	-14.9/15.1	1.069	0.111	-15.4/16.8	1.653	0.044	-10.3/21.8
H ₂ O	1.021	0.129	-14.5/15.9	1.243	0.093	-14.9/17.8	1.778	0.040	-9.9/22.3

^aGeometry was optimized in the presence of solvent at the 3D-RISM-SCF-U-DFT level.

^bThe π_a is SOMO at the ground state and the π_b is SOMO at the $\pi \rightarrow \pi$ excited state in the C_2 -symmetrical geometry. The π_1 is SOMO at the ground state and the π_2 is SOMO at the $\pi \rightarrow \pi$ excited state in the asymmetrical C_1 .

^cObserved in CH₂Cl₂; see reference [5]. In parentheses are reference [8].

Table S14: 3SA-GMC-QDPT(SAS/SAS)-calculated vertical excitation energy ΔE , oscillator strength f , and dipole moment μ_x^0 and μ_x^{ex} in the lowest energy quartet state and excited states of one-electron oxidized Re(III)-salen complexes.^{a,b}

solvent	state ^c	(Me,Me)			(OMe,OMe)			(Cl,OMe)		
		ΔE [eV]	f [au]	$\mu_x^{\text{ex}}/\mu_x^0$ [Debye]	ΔE [eV]	f [au]	$\mu_x^{\text{ex}}/\mu_x^0$ [Debye]	ΔE [eV]	f [au]	$\mu_x^{\text{ex}}/\mu_x^0$ [Debye]
		Re 5a			Re 5b			Re 5c		
none	$\pi_b \rightarrow d_{xz}$	1.463	0.544	0.0/0.0	1.300	0.640	0.0/0.0	1.344	0.551	8.2/7.1
	$\pi_a \rightarrow d_{xz}$	2.159	0.021	0.0/0.0	2.124	0.006	0.0/0.0	2.211	0.036	-1.2/7.1
CH ₂ Cl ₂	$\pi_b \rightarrow d_{xz}$	1.486	0.545	0.0/0.0	1.311	0.648	-0.1/0.1	1.328	0.504	8.9/7.8
	$\pi_a \rightarrow d_{xz}$	2.194	0.015	0.0/0.0	2.194	0.008	-0.1/0.1	2.300	0.057	-0.4/7.8
CH ₃ OH	$\pi_b \rightarrow d_{xz}$	1.533	0.547	-0.8/0.2	1.373	0.640	0.0/0.1	1.357	0.516	9.6/8.4
	$\pi_a \rightarrow d_{xz}$	2.256	0.020	-0.9/0.2	2.252	0.010	0.0/0.1	2.343	0.051	0.3/8.4
H ₂ O	$\pi_b \rightarrow d_{xz}$	1.551	0.549	-1.2/0.3	1.421	0.626	0.0/0.0	1.427	0.534	10.4/9.1
	$\pi_a \rightarrow d_{xz}$	2.279	0.025	-1.5/0.3	2.259	0.011	0.0/0.0	2.418	0.047	1.0/9.1

^aGeometry was optimized in the presence of solvent at the 3D-RISM-SCF-U-DFT level.

^bThe π_a is SOMO at the ground state and the π_b is SOMO at the $\pi \rightarrow \pi$ excited state in the C_2 -symmetrical geometry. The π_1 is SOMO at the ground state and the π_2 is SOMO at the $\pi \rightarrow \pi$ excited state in the asymmetrical C_1 .

^cIn **5c**, π_b and π_a change to π_2 and π_1 , respectively.

Table S15: NBO spin populations of one-electron oxidized salen complexes of group 10 metals in the doublet state.^{a,b}

solvent	geom.	M						Salen ligand ^c		
		nd_{xz}	nd_{yz}	nd_{z^2}	$nd_{x^2-y^2}$	nd_{xy}	$(n+1)s$	sides-1+2	side-1	side-2
Ni 2a										
none	C_2	0.085	0.006	0.003	0.000	-0.001	-0.005	0.882	0.441	0.441
CH ₂ Cl ₂	C_2 -like	0.088 (0.089 ^d)	0.006 (0.006)	0.004 (0.003)	0.000 (0.000)	-0.001 (-0.001)	-0.005 (-0.005)	0.878 (0.878)	0.437 (0.439)	0.441 (0.439)
CH ₃ OH	C_2 -like	0.094 (0.092)	0.006 (0.006)	0.003 (0.003)	0.001 (0.000)	0.000 (0.000)	-0.005 (-0.005)	0.871 (0.874)	0.431 (0.437)	0.440 (0.437)
H ₂ O	C_1	0.066 (0.093)	0.005 (0.006)	0.001 (0.003)	0.000 (0.000)	0.002 (0.000)	-0.004 (-0.005)	0.898 (0.872)	0.134 (0.436)	0.764 (0.436)
Pd 4a										
none	C_2 -like	0.069 (0.070)	0.004 (0.004)	0.007 (0.006)	0.001 (0.001)	-0.002 (-0.003)	-0.004 (-0.004)	0.895 (0.896)	0.447 (0.448)	0.448 (0.448)
CH ₂ Cl ₂	C_2 -like	0.072 (0.074)	0.004 (0.004)	0.008 (0.006)	0.001 (0.000)	-0.002 (-0.002)	-0.004 (-0.004)	0.891 (0.890)	0.434 (0.445)	0.457 (0.445)
CH ₃ OH	C_1	0.061 (0.075)	0.004 (0.004)	0.006 (0.006)	0.001 (0.001)	-0.001 (-0.002)	-0.003 (-0.003)	0.902 (0.888)	0.157 (0.444)	0.745 (0.444)
H ₂ O	C_1	0.045 (0.076)	0.003 (0.004)	0.004 (0.006)	0.001 (0.001)	-0.001 (-0.002)	-0.003 (-0.004)	0.920 (0.888)	0.062 (0.444)	0.858 (0.444)
Pt 6a										
none	C_2	0.164	0.009	0.010	0.002	0.001	-0.005	0.794	0.397	0.397
CH ₂ Cl ₂	C_2 -like	0.171 (0.171)	0.009 (0.008)	0.011 (0.010)	0.002 (0.001)	0.002 (0.002)	-0.005 (-0.005)	0.785 (0.788)	0.390 (0.394)	0.395 (0.394)
CH ₃ OH	C_2 -like	0.176 (0.175)	0.008 (0.008)	0.010 (0.010)	0.002 (0.001)	0.002 (0.002)	-0.005 (-0.005)	0.781 (0.784)	0.389 (0.392)	0.392 (0.392)
H ₂ O	C_2 -like	0.178 (0.177)	0.008 (0.008)	0.009 (0.009)	0.002 (0.001)	0.002 (0.002)	-0.005 (-0.005)	0.779 (0.780)	0.386 (0.390)	0.393 (0.390)

^aCalculated by the U-DFT and 3D-RISM-SCF-U-DFT with M06 functional.

^bSide-1 and 2 represent (PhO+CN)¹ and (PhO+CN)² moieties, respectively; see Scheme 2a for (PhO+CN)¹ and (PhO+CN)² moieties.

^cThe spin populations on the (PhO+CN)¹ and (PhO+CN)² moieties are calculated as the sum of their site-components, respectively.

^dIn parentheses are calculated at the C_2 -symmetrical geometry.

Table S16: NBO charges of one-electron oxidized salen complexes of group 10 metals in the doublet state.^{a,b}

solvent	geom.	charge		M				Salen ligand ^c			
		M	nd_{xz}	nd_{yz}	population	nd_{z^2}	$nd_{x^2-y^2}$	nd_{xy}	$(n+1)s$	sides-1+2	side-1
Ni 2a											
none	C_2	1.025	1.901	1.939	1.949	1.984	0.846	0.339	-0.694	-0.347	-0.347
CH ₂ Cl ₂	C_2 -like	1.029 (1.031 ^d)	1.897 (1.897)	1.938 (1.940)	1.949 (1.949)	1.985 (1.985)	0.848 (0.845)	0.339 (0.339)	-0.691 (-0.702)	-0.352 (-0.351)	-0.349 (-0.351)
CH ₃ OH	C_2 -like	1.026 (1.030)	1.892 (1.894)	1.941 (1.941)	1.949 (1.949)	1.984 (1.985)	0.852 (0.847)	0.341 (0.339)	-0.706 (-0.710)	-0.356 (-0.355)	-0.350 (-0.355)
H ₂ O	C_1	1.021 (1.028)	1.918 (1.893)	1.941 (1.943)	1.935 (1.949)	1.985 (1.985)	0.847 (0.849)	0.340 (0.339)	-0.715 (-0.720)	-0.599 (-0.360)	-0.116 (-0.360)
Pd 4a											
none	C_2 -like	0.876 (0.877)	1.913 (1.914)	1.920 (1.923)	1.923 (1.924)	1.981 (1.982)	1.006 (1.001)	0.369 (0.368)	-0.557 (-0.558)	-0.279 (-0.279)	-0.278 (-0.279)
CH ₂ Cl ₂	C_2 -like	0.877 (0.879)	1.910 (1.908)	1.920 (1.924)	1.923 (1.924)	1.982 (1.982)	1.009 (1.003)	0.368 (0.367)	-0.562 (-0.564)	-0.289 (-0.282)	-0.273 (-0.282)
CH ₃ OH	C_1	0.863 (0.875)	1.921 (1.908)	1.921 (1.925)	1.923 (1.924)	1.982 (1.982)	1.008 (1.006)	0.369 (0.369)	-0.559 (-0.570)	-0.484 (-0.285)	-0.075 (-0.285)
H ₂ O	C_1	0.849 (0.871)	1.937 (1.907)	1.924 (1.927)	1.925 (1.924)	1.982 (1.982)	1.004 (1.007)	0.369 (0.370)	-0.557 (-0.580)	-0.573 (-0.290)	0.016 (-0.290)
Pt 6a											
none	C_2	1.023	1.802	1.872	1.856	1.961	0.921	0.548	-0.708	-0.354	-0.354
CH ₂ Cl ₂	C_2 -like	1.025 (1.025)	1.795 (1.795)	1.873 (1.875)	1.855 (1.856)	1.961 (1.963)	0.925 (0.922)	0.549 (0.547)	-0.714 (-0.714)	-0.359 (-0.357)	-0.355 (-0.357)
CH ₃ OH	C_2 -like	1.022 (1.022)	1.790 (1.791)	1.877 (1.877)	1.855 (1.856)	1.961 (1.963)	0.925 (0.924)	0.552 (0.550)	-0.722 (-0.722)	-0.362 (-0.361)	-0.360 (-0.361)
H ₂ O	C_2 -like	1.018 (1.018)	1.788 (1.790)	1.880 (1.880)	1.855 (1.856)	1.961 (1.963)	0.926 (0.926)	0.553 (0.552)	-0.729 (-0.728)	-0.368 (-0.364)	-0.361 (-0.364)

^aCalculated by the U-DFT and 3D-RISM-SCF-U-DFT with M06 functional.

^bSide-1 and 2 represent (PhO+CN)¹ and (PhO+CN)² moieties, respectively; see Scheme 2a for (PhO+CN)¹ and (PhO+CN)² moieties.

^cThe NBO charges on the (PhO+CN)¹ and (PhO+CN)² moieties are calculated as the sum of their site-components, respectively.

^dIn parentheses are calculated at the C_2 -symmetrical geometry.

Table S17: α - and β -spin populations of one-electron oxidized salen complexes of group 10 metals in the doublet state.^{a,b}

solvent	geom.	M					
		nd_{xz}	nd_{yz}	nd_{z^2}	$nd_{x^2-y^2}$	nd_{xy}	$(n+1)s$
		Ni 2a					
none	C_2	0.993,0.908	0.973,0.968	0.976,0.973	0.992,0.992	0.422,0.423	0.168,0.173
CH_2Cl_2	C_2 -like	0.993,0.905 (0.993,0.904) ^c	0.972,0.966 (0.973,0.967)	0.976,0.972 (0.976,0.973)	0.993,0.992 (0.993,0.992)	0.423,0.425 (0.422,0.423)	0.167,0.172 (0.167,0.172)
CH_3OH	C_2 -like	0.993,0.889 (0.993,0.901)	0.973,0.968 (0.974,0.968)	0.976,0.973 (0.976,0.973)	0.992,0.992 (0.993,0.992)	0.426,0.426 (0.424,0.424)	0.168,0.173 (0.167,0.172)
H_2O	C_1	0.992,0.926 (0.993,0.900)	0.973,0.968 (0.974,0.968)	0.968,0.967 (0.976,0.973)	0.992,0.992 (0.993,0.992)	0.424,0.423 (0.425,0.425)	0.167,0.172 (0.167,0.172)
		Pd 4a					
none	C_2 -like	0.991,0.922 (0.992,0.922)	0.962,0.958 (0.963,0.959)	0.965,0.958 (0.965,0.959)	0.991,0.990 (0.991,0.991)	0.502,0.504 (0.499,0.502)	0.183,0.186 (0.182,0.186)
CH_2Cl_2	C_2 -like	0.991,0.919 (0.992,0.917)	0.962,0.958 (0.964,0.960)	0.965,0.958 (0.965,0.959)	0.991,0.990 (0.991,0.991)	0.503,0.506 (0.501,0.503)	0.182,0.186 (0.182,0.186)
CH_3OH	C_1	0.991,0.930 (0.991,0.916)	0.963,0.959 (0.965,0.961)	0.965,0.959 (0.965,0.959)	0.991,0.991 (0.991,0.991)	0.503,0.505 (0.502,0.504)	0.183,0.186 (0.183,0.186)
H_2O	C_1	0.991,0.946 (0.992,0.916)	0.964,0.961 (0.966,0.962)	0.964,0.960 (0.965,0.959)	0.991,0.991 (0.991,0.991)	0.502,0.503 (0.503,0.504)	0.183,0.186 (0.183,0.187)
		Pt 6a					
none	C_2	0.983,0.819	0.940,0.932	0.933,0.923	0.981,0.979	0.461,0.460	0.272,0.277
CH_2Cl_2	C_2 -like	0.982,0.812 (0.983,0.812)	0.941,0.932 (0.942,0.933)	0.933,0.922 (0.933,0.923)	0.981,0.980 (0.982,0.981)	0.463,0.462 (0.462,0.460)	0.272,0.277 (0.271,0.276)
CH_3OH	C_2 -like	0.983,0.807 (0.983,0.808)	0.943,0.934 (0.943,0.935)	0.932,0.923 (0.933,0.923)	0.981,0.980 (0.982,0.981)	0.464,0.462 (0.463,0.461)	0.274,0.278 (0.272,0.277)
H_2O	C_2 -like	0.983,0.805 (0.983,0.806)	0.944,0.936 (0.944,0.936)	0.932,0.923 (0.932,0.923)	0.981,0.980 (0.982,0.981)	0.464,0.462 (0.464,0.462)	0.274,0.279 (0.274,0.278)

^aCalculated by the U-DFT and 3D-RISM-SCF-U-DFT with M06 functional.

^bThe first and second values represent the α - and β -spin populations, respectively.

^cIn parentheses are calculated at the C_2 -symmetrical geometry.

Table S18: Effective **M-O** and **M-N** bond orders of one-electron oxidized salen complexes of (A) group 10 metals with the doublet state and (B) the group 7 analogues with the quartet state.^{a,b}

M		M-O¹ bond		M-O² bond		M-N¹ bond		M-N² bond	
		total	α/β	total	α/β	total	α/β	total	α/β
(A) Group 10 metal									
Ni	2a	0.34	0.16/0.18	0.34	0.16/0.18	0.42	0.20/0.22	0.42	0.20/0.22
Pd	4a	0.33	0.15/0.18	0.33	0.15/0.18	0.45	0.22/0.23	0.45	0.22/0.23
Pt	6a	0.40	0.17/0.23	0.40	0.17/0.23	0.53	0.25/0.28	0.53	0.25/0.28
(B) Group 7 metal									
Mn	1a	0.63 (0.51 ^c)	0.43/0.20 (0.34/0.17)	0.39 (0.51)	0.25/0.14 (0.34/0.17)	0.50 (0.44)	0.27/0.23 (0.23/0.21)	0.37 (0.44)	0.19/0.18 (0.23/0.21)
Tc	3a	0.68 (0.60)	0.49/0.19 (0.41/0.19)	0.51 (0.60)	0.34/0.17 (0.41/0.19)	0.56 (0.53)	0.32/0.24 (0.29/0.24)	0.48 (0.53)	0.25/0.23 (0.29/0.24)
Re	5a	0.72	0.45/0.27	0.72	0.45/0.27	0.60	0.31/0.29	0.60	0.31/0.29

^aCalculated for the complexes with (Me, Me) substituents in gas phase by the U-DFT with M06 functional.

^bWiberg bond index is employed.

^cIn parentheses are calculated at the C_2 -symmetrical geometry.

Table S19: U-TDDFT-calculated vertical excitation energy, ΔE , and oscillator strength, f , in the doublet ground and excited states of one-electron oxidized Re(III)-salen complexes.^{a,b,c}

solvent	main config. ^d	(Me,Me)		(OMe,OMe)		(Cl,OMe)	
		ΔE [eV]	f [au]	ΔE [eV]	f [au]	ΔE [eV]	f [au]
		Re 5a		Re 5b		Re 5c	
none	$d_{z^2} \rightarrow d_{yz}$	0.129	0.000	0.096	0.000	0.112	0.000
	$d_{z^2} \rightarrow d_{xz}$	0.702	0.000	0.806	0.000	0.784	0.000
	$d_{yz} \rightarrow d_{xz}$	1.043	0.002	1.194	0.003	1.160	0.004
	$d_{z^2} \rightarrow d_{x^2-y^2}$	1.133	0.000	1.008	0.000	1.007	0.000
	$\pi_b \rightarrow d_{yz}$	1.369	0.000	0.924	0.000	0.969	0.000
	$\pi_a \rightarrow d_{yz}$	1.570	0.019	1.115	0.013	1.356	0.016
	$\pi_b \rightarrow d_{xz}$	2.344	0.105	2.370	0.242	2.354	0.163
	$\pi_a \rightarrow d_{xz}$	2.637	0.002	2.633	0.005	2.785	0.012
CH ₂ Cl ₂	$d_{z^2} \rightarrow d_{yz}$	0.117	0.000	0.097	0.000	0.124	0.000
	$d_{z^2} \rightarrow d_{xz}$	0.637	0.000	0.801	0.000	0.730	0.000
	$d_{yz} \rightarrow d_{xz}$	1.031	0.001	1.226	0.004	1.132	0.004
	$d_{z^2} \rightarrow d_{x^2-y^2}$	1.140	0.000	0.967	0.000	1.026	0.000
	$\pi_b \rightarrow d_{yz}$	1.476	0.000	1.124	0.001	1.175	0.000
	$\pi_a \rightarrow d_{yz}$	1.683	0.016	1.333	0.010	1.632	0.015
CH ₃ OH	$d_{z^2} \rightarrow d_{yz}$	0.137	0.000	0.097	0.000	0.087	0.000
	$d_{z^2} \rightarrow d_{xz}$	0.729	0.000	0.786	0.000	0.743	0.000
	$d_{yz} \rightarrow d_{xz}$	0.998	0.000	1.219	0.004	1.192	0.004
	$d_{z^2} \rightarrow d_{x^2-y^2}$	1.142	0.002	0.990	0.000	0.964	0.000
	$\pi_b \rightarrow d_{yz}$	1.603	0.000	1.292	0.002	1.316	0.001
	$\pi_a \rightarrow d_{yz}$	1.801	0.013	1.487	0.010	1.798	0.017
H ₂ O	$d_{z^2} \rightarrow d_{yz}$	0.091	0.000	0.101	0.000	0.101	0.000
	$d_{z^2} \rightarrow d_{xz}$	0.725	0.000	0.787	0.000	0.731	0.000
	$d_{yz} \rightarrow d_{xz}$	1.019	0.000	1.236	0.004	1.193	0.004
	$d_{z^2} \rightarrow d_{x^2-y^2}$	1.150	0.002	0.980	0.000	0.995	0.000
	$\pi_b \rightarrow d_{yz}$	1.622	0.000	1.384	0.000	1.426	0.001
	$\pi_a \rightarrow d_{yz}$	1.831	0.017	1.575	0.008	1.911	0.010

^aCalculated by the U-TDDFT and 3D-RISM-U-TDDFT with M06 functional.

^bGeometry was optimized in the presence of solvent at the 3D-RISM-SCF-U-DFT level.

^cThe doublet ground state has a main electron configuration consisting of a closed-shell singlet electron configuration of [salen]²⁻ and a doublet electronic configuration of Re(IV) with d_{z^2} DOMO and d_{yz} SOMO.

^dIn **5c**, π_b and π_a change to π_1 and π_2 , respectively.

Table S20: 9SA-GMC-QDPT(SAS2/SAS2)-calculated vertical excitation energy ΔE , oscillator strength f , and dipole moment μ_x^{gr} and μ_x^{ex} in the doublet ground and excited states of one-electron oxidized Re(III)-salen complexes.^{a,b}

solvent	main config.	(Me,Me)			(OMe,OMe)		
		ΔE [eV]	f [au]	$\mu_x^{\text{ex}}/\mu_x^{\text{gr}}$ [Debye]	ΔE [eV]	f [au]	$\mu_x^{\text{ex}}/\mu_x^{\text{gr}}$ [Debye]
		Re 5a			Re 5b		
none	$d_{z^2} \rightarrow d_{yz}$	0.398	0.000	0.0/0.0	0.340	0.000	0.0/0.0
	$\pi_b \rightarrow d_{yz}$	1.221	0.000	0.0/0.0	0.860	0.000	0.0/0.0
	$\pi_a \rightarrow d_{yz}$	1.722	0.077	0.0/0.0	1.393	0.146	0.0/0.0
	$\pi_b \rightarrow d_{xz}$	2.239	0.289	0.0/0.0	2.184	0.200	0.0/0.0
	$\pi_a \rightarrow d_{xz}$	2.866	0.004	0.0/0.0	2.668	0.006	0.0/0.0
CH ₂ Cl ₂	$d_{z^2} \rightarrow d_{yz}$	0.346	0.000	0.0/0.0	0.225	0.000	0.0/0.0
	$\pi_b \rightarrow d_{yz}$	1.276	0.000	0.0/0.0	0.950	0.000	0.0/0.0
	$\pi_a \rightarrow d_{yz}$	1.764	0.059	0.0/0.0	1.543	0.189	0.0/0.0
	$\pi_b \rightarrow d_{xz}$	2.144	0.276	0.0/0.0	2.231	0.240	0.0/0.0
	$\pi_a \rightarrow d_{xz}$	2.805	0.005	0.0/0.0	2.741	0.007	0.0/0.0
CH ₃ OH	$d_{z^2} \rightarrow d_{yz}$	0.299	0.000	0.0/0.0	0.180	0.000	0.0/0.0
	$\pi_b \rightarrow d_{yz}$	1.336	0.001	-0.1/0.0	1.051	0.000	-0.2/0.0
	$\pi_a \rightarrow d_{yz}$	1.731	0.089	0.0/0.0	1.568	0.224	0.1/0.0
	$\pi_b \rightarrow d_{xz}$	2.223	0.301	0.1/0.0	2.247	0.272	0.1/0.0
	$\pi_a \rightarrow d_{xz}$	2.891	0.004	-0.1/0.0	2.778	0.008	-0.1/0.0
H ₂ O	$d_{z^2} \rightarrow d_{yz}$	0.235	0.000	0.1/0.1	0.147	0.000	0.0/0.1
	$\pi_b \rightarrow d_{yz}$	1.419	0.002	-0.2/0.1	1.107	0.002	-0.3/0.1
	$\pi_a \rightarrow d_{yz}$	1.666	0.112	0.1/0.1	1.585	0.265	0.2/0.1
	$\pi_b \rightarrow d_{xz}$	2.310	0.337	0.3/0.1	2.259	0.290	0.2/0.1
	$\pi_a \rightarrow d_{xz}$	3.006	0.002	-0.2/0.1	2.807	0.008	-0.2/0.1

^aGeometry was optimized in the presence of solvent at the 3D-RISM-SCF-U-DFT level.

^bThe doublet ground state has a main electron configuration consisting of a closed-shell singlet electron configuration of [salen]²⁻ and a doublet electronic configuration of Re(IV) with d_{z^2} DOMO and d_{yz} SOMO.

Table S21: NBO spin populations of one-electron oxidized salen complexes of group 7 metals in the quartet state.^{a,b}

solvent	geom.	M					Salen ligand ^c			
		nd_{xz}	nd_{yz}	nd_{z^2}	$nd_{x^2-y^2}$	nd_{xy}	$(n+1)s$	sides-1+2	side-1	side-2
Mn 1a										
none	C_1	-0.803 (-0.805 ^d)	-0.874 (-0.890)	-0.927 (-0.928)	-0.878 (-0.879)	-0.246 (-0.239)	-0.053 (-0.053)	0.745 (0.754)	-0.032 (0.377)	0.777 (0.377)
CH ₂ Cl ₂	C_1	-0.811 (-0.811)	-0.880 (-0.893)	-0.928 (-0.929)	-0.881 (-0.882)	-0.248 (-0.242)	-0.052 (-0.052)	0.766 (0.772)	-0.081 (0.386)	0.847 (0.386)
CH ₃ OH	C_1	-0.824 (-0.820)	-0.890 (-0.898)	-0.929 (-0.929)	-0.887 (-0.887)	-0.251 (-0.243)	-0.049 (-0.050)	0.797 (0.794)	-0.080 (0.397)	0.877 (0.397)
H ₂ O	C_1	-0.830 (-0.824)	-0.893 (-0.900)	-0.929 (-0.929)	-0.890 (-0.891)	-0.252 (-0.245)	-0.049 (-0.049)	0.811 (0.804)	-0.077 (0.402)	0.888 (0.402)
Tc 3a										
none	C_1	-0.592 (-0.579)	-0.776 (-0.799)	-0.853 (-0.857)	-0.811 (-0.806)	-0.086 (-0.083)	-0.108 (-0.109)	0.210 (0.214)	-0.268 (0.107)	0.478 (0.107)
CH ₂ Cl ₂	C_1	-0.608 (-0.577)	-0.794 (-0.808)	-0.855 (-0.857)	-0.813 (-0.807)	-0.089 (-0.084)	-0.106 (-0.106)	0.251 (0.224)	-0.277 (0.112)	0.528 (0.112)
CH ₃ OH	C_1	-0.629 (-0.577)	-0.812 (-0.817)	-0.857 (-0.858)	-0.817 (-0.809)	-0.091 (-0.084)	-0.103 (-0.103)	0.294 (0.236)	-0.272 (0.118)	0.566 (0.118)
H ₂ O	C_1	-0.648 (-0.578)	-0.820 (-0.821)	-0.858 (-0.859)	-0.821 (-0.811)	-0.092 (-0.084)	-0.102 (-0.102)	0.326 (0.242)	-0.277 (0.121)	0.603 (0.121)
Re 5a										
none	C_2	-0.341	-0.730	-0.795	-0.766	-0.046	-0.171	-0.146	-0.073	-0.073
CH ₂ Cl ₂	C_2	-0.340	-0.733	-0.807	-0.771	-0.049	-0.173	-0.120	-0.060	-0.060
CH ₃ OH	C_2 -like	-0.325 (-0.325)	-0.742 (-0.742)	-0.810 (-0.810)	-0.772 (-0.772)	-0.048 (-0.048)	-0.172 (-0.169)	-0.121 (-0.120)	-0.062 (-0.060)	-0.059 (-0.060)
H ₂ O	C_2 -like	-0.315 (-0.315)	-0.746 (-0.746)	-0.812 (-0.812)	-0.777 (-0.777)	-0.048 (-0.048)	-0.171 (-0.169)	-0.121 (-0.120)	-0.061 (-0.060)	-0.060 (-0.060)

^aCalculated by the U-DFT and 3D-RISM-SCF-U-DFT with M06 functional.

^bSide-1 and 2 represent (PhO+CN)¹ and (PhO+CN)² moieties, respectively; see Scheme 2a for (PhO+CN)¹ and (PhO+CN)² moieties.

^cThe spin populations on the (PhO+CN)¹ and (PhO+CN)² moieties are calculated as the sum of their site-components, respectively.

^dIn parentheses are calculated at the C_2 -symmetrical geometry.

Table S22: NBO charges of one-electron oxidized salen complexes of group 7 metals in the quartet state.^{a,b}

solvent	geom.	charge			M				Salen ligand ^c		
		M	nd_{xz}	nd_{yz}	population	nd_{z^2}	$nd_{x^2-y^2}$	nd_{xy}	$(n+1)s$	sides-1+2	side-1
Mn 1a											
none	C_1	1.549 (1.561 ^d)	1.149 (1.143)	1.081 (1.068)	1.038 (1.038)	1.094 (1.095)	0.812 (0.813)	0.246 (0.247)	-0.369 (-0.386)	-0.357 (-0.193)	-0.012 (-0.193)
CH ₂ Cl ₂	C_1	1.565 (1.578)	1.144 (1.135)	1.075 (1.064)	1.038 (1.039)	1.091 (1.092)	0.813 (0.815)	0.244 (0.245)	-0.360 (-0.378)	-0.409 (-0.189)	0.049 (-0.189)
CH ₃ OH	C_1	1.596 (1.604)	1.134 (1.124)	1.066 (1.059)	1.039 (1.040)	1.087 (1.086)	0.813 (0.816)	0.239 (0.240)	-0.380 (-0.394)	-0.459 (-0.197)	0.079 (-0.197)
H ₂ O	C_1	1.608 (1.614)	1.129 (1.120)	1.063 (1.058)	1.039 (1.041)	1.083 (1.083)	0.813 (0.817)	0.237 (0.238)	-0.392 (-0.402)	-0.486 (-0.201)	0.094 (-0.201)
Tc 3a											
none	C_1	1.484 (1.508)	1.185 (1.173)	1.135 (1.117)	1.036 (1.034)	1.147 (1.152)	0.721 (0.724)	0.274 (0.273)	-0.302 (-0.328)	-0.251 (-0.164)	-0.051 (-0.164)
CH ₂ Cl ₂	C_1	1.514 (1.538)	1.177 (1.153)	1.117 (1.107)	1.037 (1.037)	1.146 (1.151)	0.723 (0.727)	0.270 (0.270)	-0.308 (-0.334)	-0.293 (-0.167)	-0.015 (-0.167)
CH ₃ OH	C_1	1.552 (1.571)	1.162 (1.133)	1.100 (1.098)	1.040 (1.040)	1.142 (1.149)	0.723 (0.728)	0.266 (0.266)	-0.337 (-0.356)	-0.347 (-0.178)	0.010 (-0.178)
H ₂ O	C_1	1.567 (1.585)	1.160 (1.124)	1.092 (1.094)	1.041 (1.041)	1.138 (1.148)	0.723 (0.729)	0.263 (0.264)	-0.350 (-0.368)	-0.385 (-0.184)	0.035 (-0.184)
Re 5a											
none	C_2	1.692	0.961	1.106	0.990	1.135	0.686	0.401	-0.510	-0.255	-0.255
CH ₂ Cl ₂	C_2	1.720	0.955	1.099	0.979	1.136	0.688	0.395	-0.516	-0.258	-0.258
CH ₃ OH	C_2 -like	1.754 (1.754)	0.933 (0.933)	1.090 (1.090)	0.982 (0.982)	1.135 (1.135)	0.689 (0.689)	0.392 (0.392)	-0.540 (-0.540)	-0.270 (-0.270)	-0.270 (-0.270)
H ₂ O	C_2 -like	1.767 (1.767)	0.921 (0.921)	1.087 (1.087)	0.982 (0.982)	1.140 (1.140)	0.688 (0.688)	0.390 (0.390)	-0.550 (-0.550)	-0.275 (-0.275)	-0.275 (-0.275)

^aCalculated by the U-DFT and 3D-RISM-SCF-U-DFT with M06 functional.

^bSide-1 and 2 represent (PhO+CN)¹ and (PhO+CN)² moieties, respectively; see Scheme 2a for (PhO+CN)¹ and (PhO+CN)² moieties.

^cThe NBO charges on the (PhO+CN)¹ and (PhO+CN)² moieties are calculated as the sum of their site-components, respectively.

^dIn parentheses are calculated at the C_2 -symmetrical geometry.

Table S23: α - and β -spin populations of one-electron oxidized salen complexes of group 7 metals in the quartet state.^{a,b}

solvent	geom.	M					
		nd_{xz}	nd_{yz}	nd_{z^2}	$nd_{x^2-y^2}$	nd_{xy}	$(n+1)s$
Mn 1a							
none	C_1	0.173,0.976 (0.169,0.974) ^c	0.103,0.978 (0.089,0.979)	0.055,0.982 (0.055,0.983)	0.108,0.986 (0.108,0.987)	0.283,0.529 (0.287,0.527)	0.096,0.150 (0.097,0.150)
CH ₂ Cl ₂	C_1	0.167,0.978 (0.162,0.973)	0.097,0.978 (0.085,0.978)	0.055,0.983 (0.055,0.984)	0.105,0.986 (0.105,0.987)	0.282,0.530 (0.287,0.529)	0.096,0.148 (0.096,0.148)
CH ₃ OH	C_1	0.155,0.979 (0.152,0.972)	0.088,0.978 (0.080,0.979)	0.055,0.984 (0.055,0.985)	0.100,0.987 (0.099,0.987)	0.281,0.532 (0.286,0.530)	0.095,0.144 (0.095,0.145)
H ₂ O	C_1	0.150,0.980 (0.148,0.972)	0.085,0.978 (0.079,0.979)	0.055,0.984 (0.056,0.985)	0.097,0.987 (0.096,0.987)	0.281,0.533 (0.286,0.531)	0.094,0.143 (0.094,0.143)
Tc 3a							
none	C_1	0.297,0.889 (0.297,0.876)	0.179,0.956 (0.159,0.958)	0.092,0.945 (0.088,0.945)	0.168,0.979 (0.173,0.979)	0.317,0.404 (0.321,0.404)	0.083,0.191 (0.082,0.191)
CH ₂ Cl ₂	C_1	0.284,0.892 (0.288,0.889)	0.162,0.955 (0.150,0.957)	0.091,0.946 (0.090,0.947)	0.166,0.980 (0.172,0.979)	0.317,0.406 (0.322,0.405)	0.082,0.188 (0.082,0.188)
CH ₃ OH	C_1	0.266,0.896 (0.278,0.855)	0.144,0.956 (0.140,0.958)	0.092,0.949 (0.091,0.949)	0.162,0.979 (0.170,0.979)	0.316,0.407 (0.322,0.406)	0.081,0.184 (0.081,0.185)
H ₂ O	C_1	0.256,0.904 (0.273,0.851)	0.136,0.956 (0.136,0.958)	0.091,0.950 (0.091,0.950)	0.158,0.980 (0.168,0.979)	0.316,0.408 (0.322,0.407)	0.081,0.183 (0.081,0.183)
Re 5a							
none	C_2	0.310,0.651	0.188,0.918	0.098,0.892	0.185,0.951	0.320,0.366	0.115,0.286
CH ₂ Cl ₂	C_2	0.308,0.648	0.183,0.916	0.086,0.893	0.183,0.953	0.320,0.368	0.111,0.284
CH ₃ OH	C_2 -like	0.304,0.629 (0.304,0.629)	0.174,0.916 (0.174,0.916)	0.086,0.896 (0.086,0.896)	0.182,0.954 (0.182,0.954)	0.320,0.368 (0.320,0.368)	0.110,0.282 (0.110,0.282)
H ₂ O	C_2 -like	0.303,0.618 (0.303,0.618)	0.170,0.917 (0.170,0.917)	0.085,0.897 (0.085,0.897)	0.182,0.958 (0.182,0.958)	0.320,0.368 (0.320,0.368)	0.110,0.281 (0.110,0.281)

^aCalculated by the U-DFT and 3D-RISM-SCF-U-DFT with M06 functional.

^bThe first and second values represent the α - and β -spin populations, respectively.

^cIn parentheses are calculated at the C_2 -symmetrical geometry.

Table S24: Solvent effect on α -spin π_a and π_b orbital energies and π_a - π_b energy difference of one-electron oxidized salen complexes of (A) group 10 metals and (B) group 7 analogues under the C_2 symmetry.^a

M	solvent	geom. ^b	ε_{π_a}	ε_{π_b}	$\Delta\varepsilon$	M	solvent	geom. ^b	ε_{π_a}	ε_{π_b}	$\Delta\varepsilon$		
(A) Group 10 metal						(B) Group 7 metal							
doublet state						quartet state							
Ni	2a	none	C_2	-9.07	-9.37	0.30	Mn	1a	none	C_1	-12.88	-12.84	0.04
		CH ₂ Cl ₂	C_2 -like	-7.40	-7.71	0.31			CH ₂ Cl ₂	C_1	-9.30	-9.26	0.04
		CH ₃ OH	C_2 -like	-7.17	-7.48	0.31			CH ₃ OH	C_1	-8.33	-8.29	0.04
		H ₂ O	C_1	-7.02	-7.33	0.31			H ₂ O	C_1	-8.15	-8.12	0.03
Pd	4a	none	C_2 -like	-9.02	-9.29	0.27	Tc	3a	none	C_1	-12.88	-12.69	0.19
		CH ₂ Cl ₂	C_2 -like	-7.38	-7.66	0.28			CH ₂ Cl ₂	C_1	-9.32	-9.13	0.19
		CH ₃ OH	C_1	-7.14	-7.42	0.28			CH ₃ OH	C_1	-8.41	-8.22	0.19
		H ₂ O	C_1	-6.99	-7.27	0.28			H ₂ O	C_1	-8.24	-8.05	0.19
Pt	6a	none	C_2	-9.00	-9.35	0.35	Re	5a	none	C_2	-12.98	-12.77	0.21
		CH ₂ Cl ₂	C_2 -like	-7.35	-7.71	0.36			CH ₂ Cl ₂	C_2	-9.43	-9.23	0.20
		CH ₃ OH	C_2 -like	-7.09	-7.45	0.36			CH ₃ OH	C_2 -like	-8.51	-8.31	0.20
		H ₂ O	C_2 -like	-6.95	-7.31	0.36			H ₂ O	C_2 -like	-8.35	-8.15	0.20
						doublet state							
						Re	5a	none	C_2	-13.33	-12.74	0.59	
								CH ₂ Cl ₂	C_2	-9.77	-9.18	0.59	
								CH ₃ OH	C_2	-8.83	-8.25	0.58	
								H ₂ O	C_2	-8.64	-8.06	0.58	

^aCalculated for the complexes with (Me,Me) substituents by the U-DFT and 3D-RISM-SCF-U-DFT with M06 functional. Unit is in [eV].

^bThe symmetry of geometry at the global free energy minimum.

active space of GMSCF with (19e, 18o) for π -orbitals of salen ligand

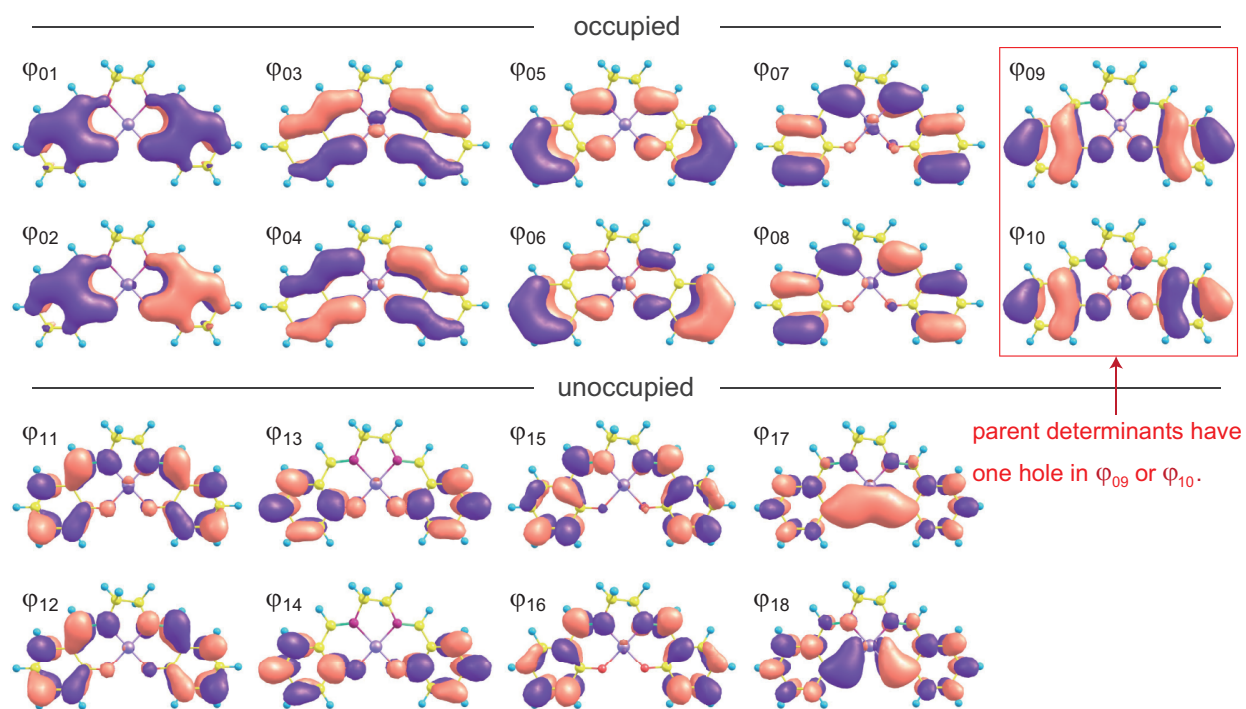
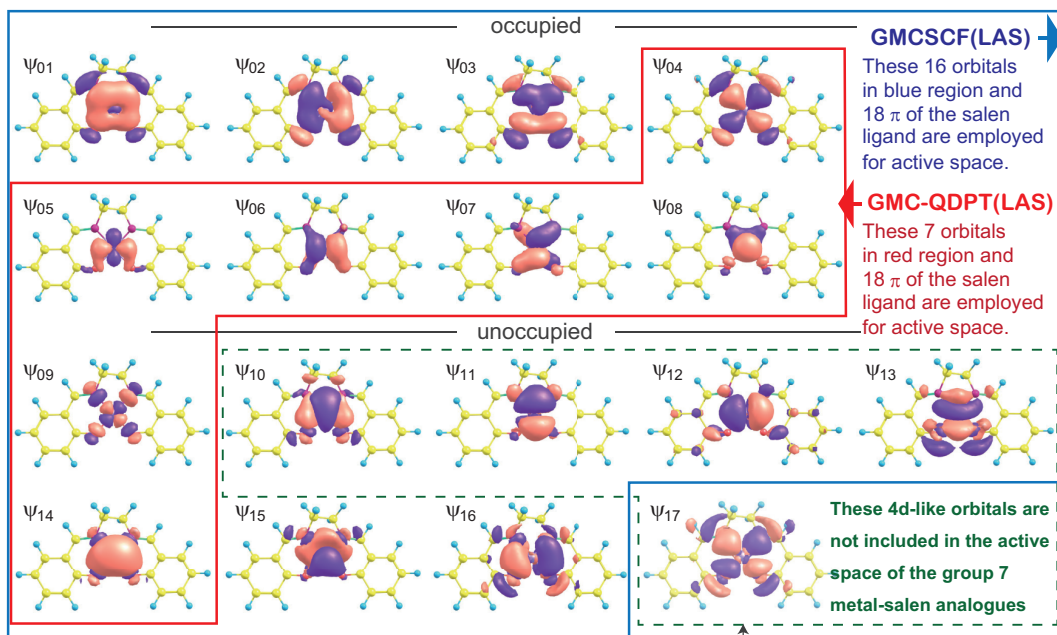


Figure S1: Selection of active space orbitals at the 2SA-GMC-QDPT(SAS/SAS) level.

(a) Active space of GMC-SCF with (34e, 34o) for the salen complexes of group 10 metals.



Also, Ψ_{17} orbital is not included in active space of GMSCSF(LAS) and GMC-QDPT(LAS/MAS) calculations.

(b) Active space of GMC-SCF with (30e, 30o) for the salen complexes of group 7 metals.

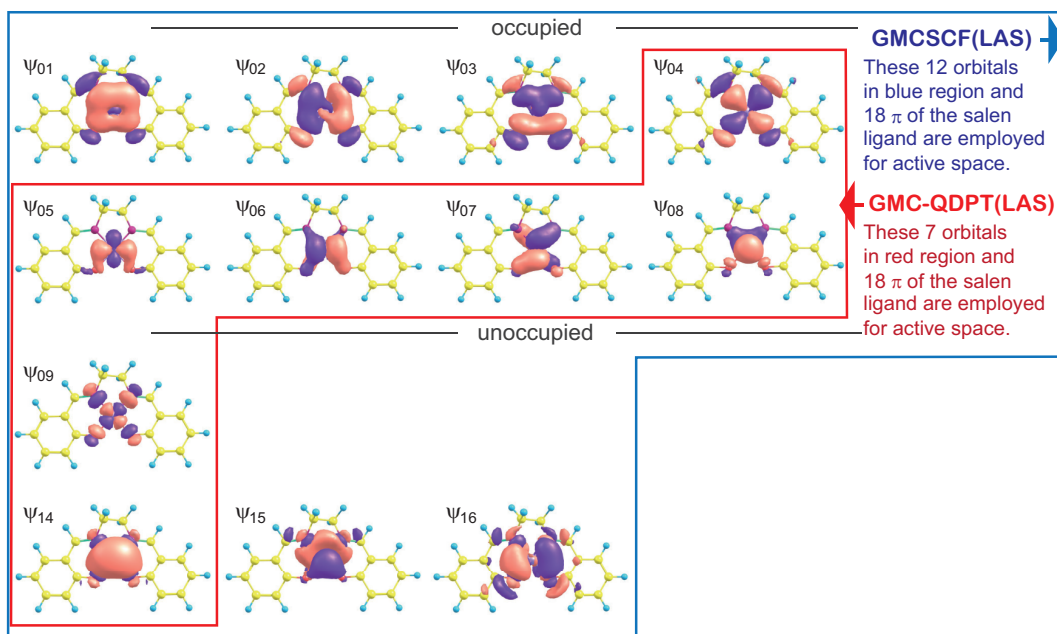


Figure S2: Selection of active space orbitals at the 2SA-GMC-QDPT(LAS/MAS) level.

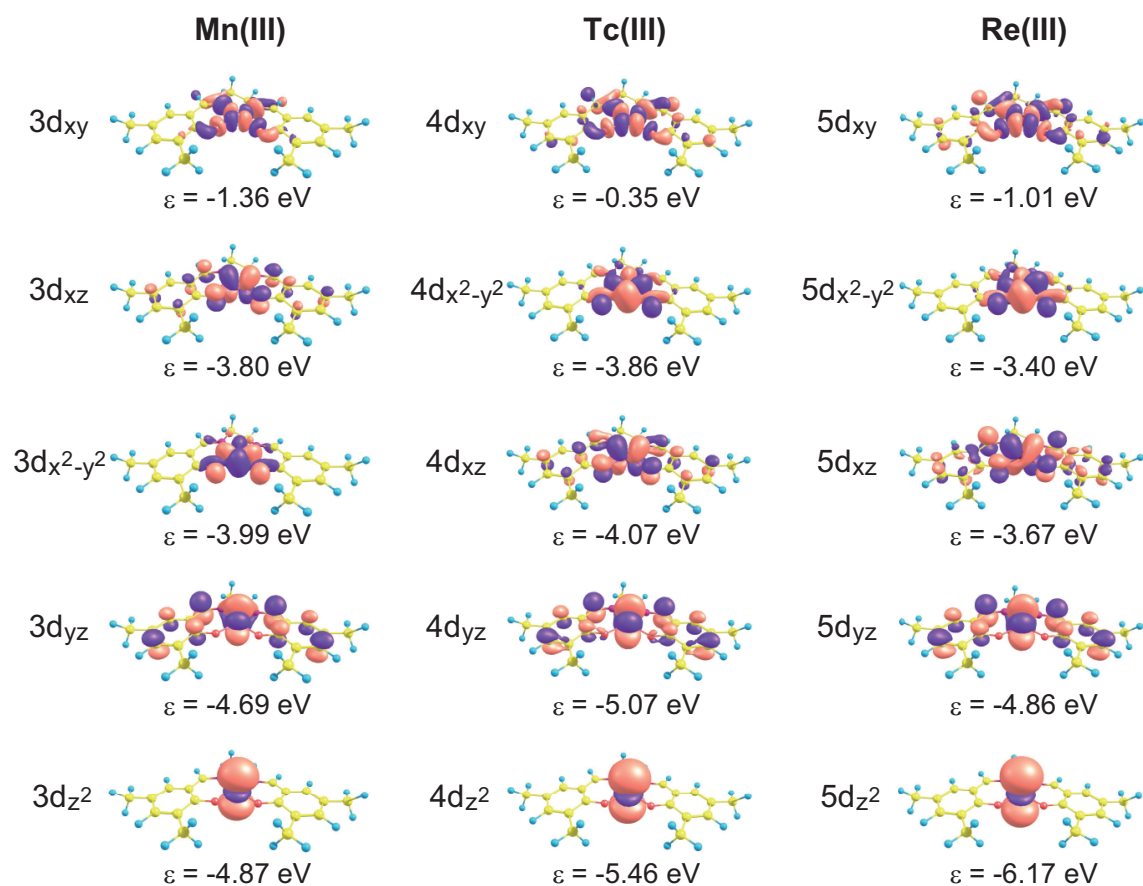


Figure S3: The d orbital energy splitting of α -spin in the quintet state of non-oxidized salen complex of group 7 metal with substituents (Me, Me) in CH_2Cl_2 .^{a,b}

^aCalculated by the U-DFT method with M06 functional. ^bThese five d orbitals are unoccupied in the α -spin space.

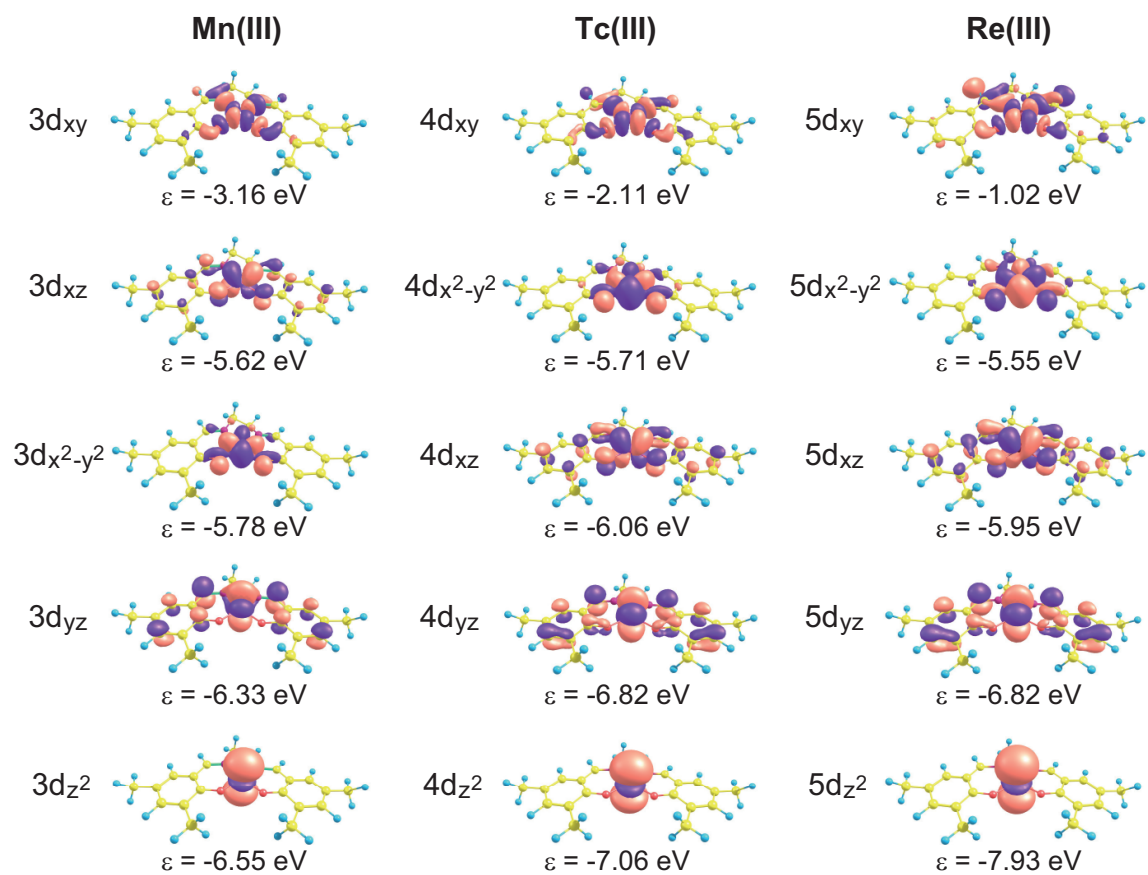
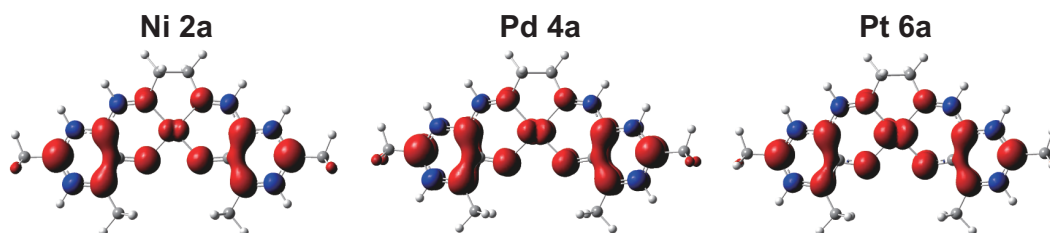


Figure S4: The d orbital energy splitting of α -spin in the quartet state of one-electron oxidized salen complex of group 7 metal with substituents (Me, Me) in CH₂Cl₂.^{a,b}

^aCalculated by the U-DFT method with M06 functional. ^bThese five d orbitals are unoccupied in the α -spin space.

(a) In CH₃OH solvent.



(b) In H₂O solvent.

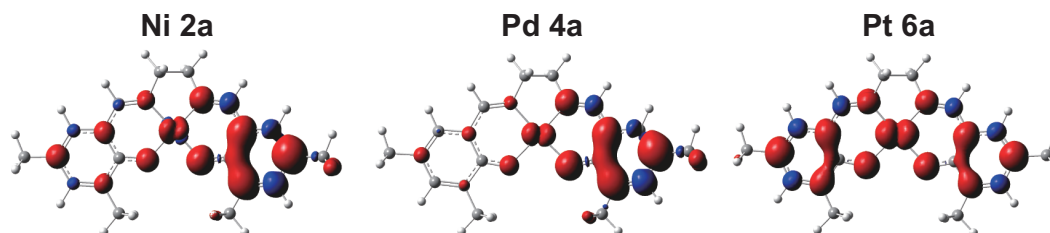


Figure S5: Distribution of total spin density of one-electron oxidized salen complexes of group 10 metals **2a**, **4a**, and **6a** in the doublet state, where the red region represents the positive total spin density and the blue region represents the negative total spin density.

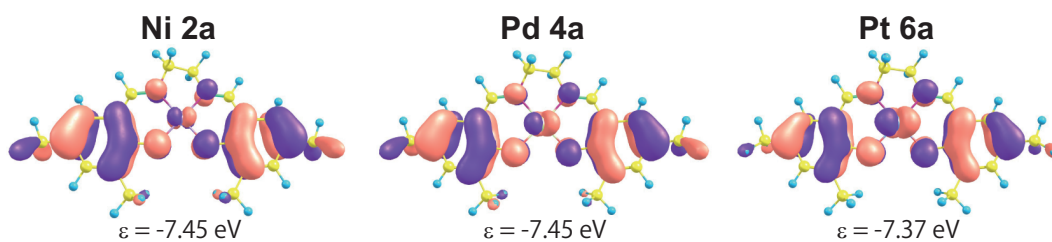
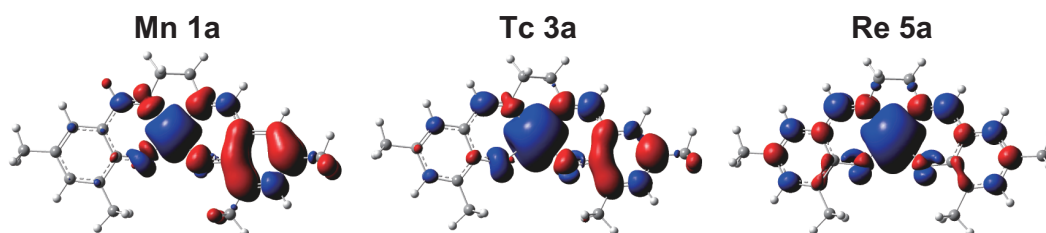


Figure S6: β -spin LUMO character of one-electron oxidized salen complexes of group 10 metals **2a**, **4a**, and **6a** with the doublet state in CH_2Cl_2 solution.

(a) In CH_3OH solvent.



(b) In H_2O solvent.

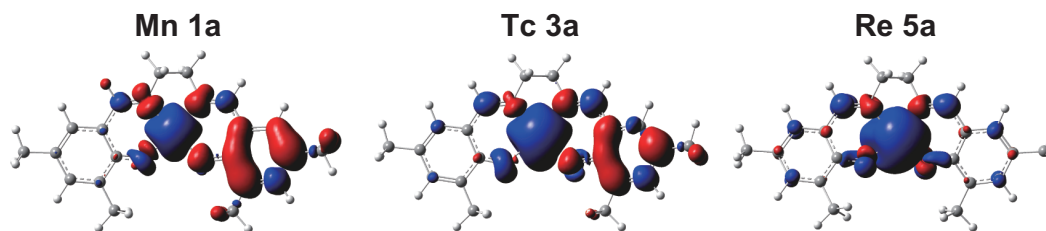


Figure S7: Distribution of total spin density of one-electron oxidized salen complexes of group 7 metals **1a**, **3a**, and **5a** with the quartet state, where the red region represents the positive total spin density and the blue region represents the negative total spin density.

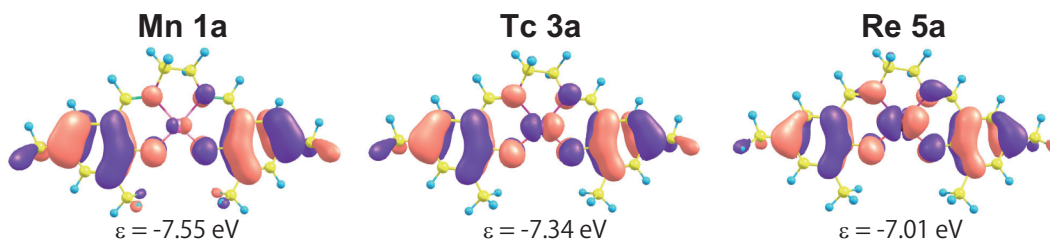


Figure S8: β -spin LUMO character of one-electron oxidized salen complexes of group 7 metals **1a**, **3a**, and **5a** with the quartet state in CH_2Cl_2 solution.^a ^aCalculated under the C_2 -symmetry.

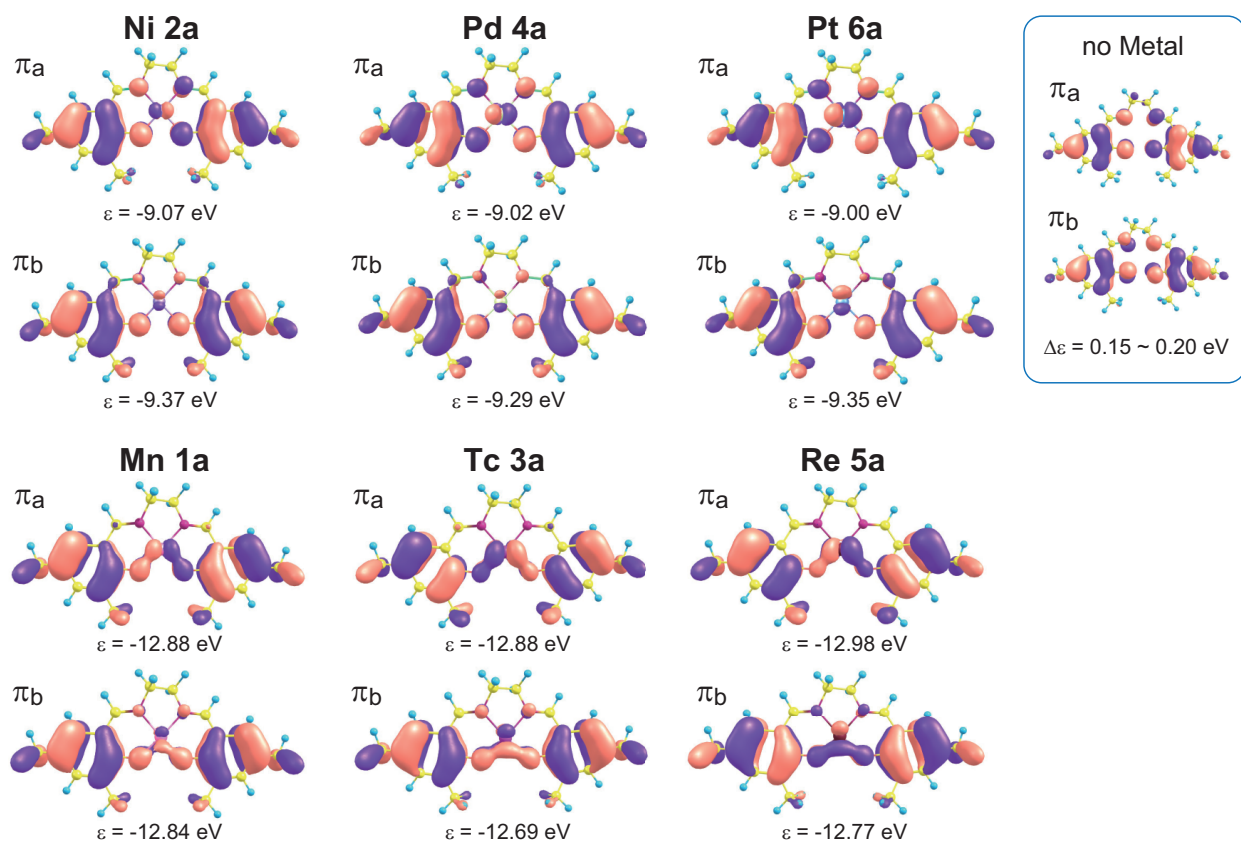


Figure S9: Shapes of α -spin π_a and π_b MOs on one-electron oxidized salen complexes of group 7 and 10 metals in gas phase.^a ^aCalculated under the C_2 -symmetry.